TKK Dissertations 147
Espoo 2008

MEASURING PHOTODARKENING FROM Yb DOPED FIBERS

Doctoral Dissertation

Joona Koponen

Helsinki University of Technology
Faculty of Electronics, Communications and Automation
Department of Micro and Nanosciences

TKK Dissertations 147
Espoo 2008

MEASURING PHOTODARKENING FROM Yb DOPED FIBERS

Doctoral Dissertation

Joona Koponen

Dissertation for the degree of Doctor of Science in Technology to be presented with due permission of the Faculty of Electronics, Communications and Automation for public examination and debate in Micronova at Helsinki University of Technology (Espoo, Finland) on the 12th of December, 2008, at 12 noon.

Helsinki University of Technology
Faculty of Electronics, Communications and Automation
Department of Micro and Nanosciences

Teknillinen korkeakoulu
Elektroniikan, tietoliikenteen ja automaation tiedekunta
Mikro- ja nanotekniikan laitos

Distribution:
Helsinki University of Technology
Faculty of Electronics, Communications and Automation
Department of Micro and Nanosciences
P.O. Box 3500 (Tietotie 3)
FI - 02015 TKK
FINLAND
URL: http://nano.tkk.fi/
Tel. +358-9-451 3121
Fax +358-9-451 3128
E-mail: joona.koponen@liekki.com

ISBN 978-951-22-9667-5
ISBN 978-951-22-9668-2 (PDF)
ISSN 1795-2239
ISSN 1795-4584 (PDF)
URL: http://lib.tkk.fi/Diss/2008/isbn9789512296682/

TKK-DISS-2540

Multiprint Oy
Espoo 2008

ABSTRACT OF DOCTORAL DISSERTATION	HELSINKI UNIVERSITY OF TECHNOLOGY P.O. BOX 1000, FI-02015 TKK http://www.tkk.fi

Author Joona Koponen

Name of the dissertation
Measuring photodarkening from Yb doped fibers

Manuscript submitted 12.9.2008	Manuscript revised 7.11.2008
Date of the defence 12.12.2008	
☐ Monograph	☒ Article dissertation (summary + original articles)

Faculty Faculty of Electronics, Communications and Automation
Department Department of Micro and Nanosciences
Field of research Photonics
Opponent(s) Dr. Lars Norin
Supervisor Prof. Seppo Honkanen
Instructor

Abstract

Yb doped fibers are used widely in applications requiring high beam quality and efficiency. A detrimental phenomenon, photodarkening, is known to reduce the efficiency of fiber devices under some operating conditions, and in extreme cases to prevent lasing altogether. Photodarkening manifests as an incrementally increasing spectrally broad transmission loss in the Yb doped core of a fiber, and it is caused by the exposure to pump- or signal photons.

This work focused on development of methods to benchmark fibers for photodarkening, and to develop methods to study the temporal and spatial characteristics of photodarkening. A measurement method for conducting benchmarking and spectral studies on single-mode fibers was developed, and a similar alternative method was developed for large-mode-area fibers. Both approaches were studied experimentally and by simulations. Additionally, an experimental setup was built to study the spatial photodarkening differences in large-mode-area fibers. Observations agreed with the simulated results.

Photodarkening rate was found to have a repeatable spectral response with fibers of similar but varying compositions, and the photodarkening induced temporal transmission loss was found to follow a stretched-exponential decay rate, and a bi-exponential decay rate. Photodarkening was found to be proportional to the inversion of a fiber sample; and also to have a 7^{th} power dependency to inversion; and more generally, to have a 7^{th} power dependency to the excited state Yb ion density.

The methodology obtained through this work enable benchmarking of Yb doped single-mode and large-mode-area fibers. The observed excited state ion density dependency to the photodarkening rate has strong implications to Yb fiber devices, as a given fiber may photodarken with a high rate in one application (having a higher inversion), and non-measurably in another application (having a lower inversion).

Keywords ytterbium, photodarkening, optical fiber, metrology

ISBN (printed) 978-951-22-9667-5	ISSN (printed) 1795-2239
ISBN (pdf) 978-951-22-9668-2	ISSN (pdf) 1795-4584
Language English	Number of pages 79 + 47

Publisher Helsinki University of Technology, Department of Micro and Nanosciences

Print distribution Helsinki University of Technology, Department of Micro and Nanosciences

☒ The dissertation can be read at http://lib.tkk.fi/Diss/2008/isbn9789512296682/

VÄITÖSKIRJAN TIIVISTELMÄ	TEKNILLINEN KORKEAKOULU PL 1000, 02015 TKK http://www.tkk.fi

Tekijä Joona Koponen

Väitöskirjan nimi
Valon aiheuttaman vaimenemisen mittaaminen Yb seostetuista kuiduista

Käsikirjoituksen päivämäärä 12.9.2008	Korjatun käsikirjoituksen päivämäärä 7.11.2008

Väitöstilaisuuden ajankohta 12.12.2008

☐ Monografia	☒ Yhdistelmäväitöskirja (yhteenveto + erillisartikkelit)

Tiedekunta	Elektroniikan, tietoliikenteen ja automaation tiedekunta
Laitos	Mikro- ja nanotekniikan laitos
Tutkimusala	Fotoniikka
Vastaväittäjä(t)	Dr. Lars Norin
Työn valvoja	Prof. Seppo Honkanen
Työn ohjaaja	

Tiivistelmä

Yb seostettuja kuituja käytetään laajasti sovelluksissa, joissa tarvitaan hyvää säteenlaatua ja hyötysuhdetta. Valon aiheuttama vaimeneminen, photodarkening, on haitallinen ilmiö joka vähentää lasereiden ja vahvistimien tehokkuutta ja elinikää. Valon aiheuttama vaimeneminen havaitaan ajan kuluessa lisääntyvänä spektraalisesti leveänä häviönä Yb seostettujen kuitujen ytimissä. Vaimenemisen aiheuttaa seostetun lasin altistuminen pumppu- tai signaalisäteilylle.

Väitöskirja käsittelee menetelmiä mitata ja vertailla valon aiheuttamaa häviötä eri kokoisissa Yb seostetuissa kuiduissa. Soveltuvat menetelmät kehitettiin yksimuotokuiduille sekä monimuotokuiduille. Aihetta tutkittiin simuloimalla sekä kokeellisesti. Lisäksi tutkittiin valon aiheuttaman häviön eroja ytimen poikkileikkauksen eri kohdissa tilanteessa, jossa poikkileikkauksen inversiojakauma ei ole tasainen.

Valon aiheuttaman häviön spektraalisen vasteen havaittiin olevan samankaltainen useilla tutkituilla lasimateriaaleilla. Häviön aikavaste voitiin määrittää venytetyllä eksponenttifuntiolla sekä kaksoiseksponenttifunktiolla. Aikavastetta mitattiin eri inversiotasoilla. Tulokset osoittivat häviön kasvamisen nopeuden olevan suhteessa inversion seitsemänteen potenssiin, sekä yleisemmin virittyneiden Yb ionien tiheyden seitsemänteen potenssiin.

Työssä kehitetyt menetelmät mahdollistavat Yb seostettujen kuitujen valon aiheuttaman vaimenemisen vertailun. Menetelmät toimivat sekä yksimuotokuidussa, että monimuotokuiduissa. Havaittu virittyneiden Yb ionien tiheyden vaikutus vaimenemisen kasvun nopeuteen selittää monia eri kuitujen käyttötarkoituksissa havaittuja eroja: korkean inversion käyttötarkoituksissa vaimennus kasvaa nopeammin kuin matalan inversion käyttötarkoituksissa, vaikka käytetyn Yb seostetun lasin kyky vaimentua olisi sama.

Asiasanat ytterbium, photodarkening, optinen kuitu, mittaustekniikka

ISBN (painettu) 978-951-22-9667-5	ISSN (painettu) 1795-2239
ISBN (pdf) 978-951-22-9668-2	ISSN (pdf) 1795-4584
Kieli englanti	Sivumäärä 79 + 47

Julkaisija Teknillinen korkeakoulu, Mikro- ja nanotekniikan laitos

Painetun väitöskirjan jakelu Teknillinen korkeakoulu, Mikro- ja nanotekniikan laitos

☒ Luettavissa verkossa osoitteessa http://lib.tkk.fi/Diss/2008/isbn9789512296682/

Preface

The work presented in this thesis was done in Liekki Oy during the years 2006-2008, and many people were involved in the process. Especially I would like to thank the product development team members that were present during the early part of the work, namely Dr. Simo Tammela, Mikko Söderlund, and Dr. Hanna Hoffman for the fruitful discussions on photodarkening, fibers, and everything. I thank Dr. Mircea Hotoleanu for all his support on my simulation needs, such as digging out the inversion levels from LAD during the time that no such option was available in the user interface. Both Marko Laurila and Teemu Kokki deserve thanks and praise for their help with the latest experiments. I'm grateful for all the help and advice I received from Dr. Valery Filippov and Hong Po on doped fibers and fiber laser/amplifier specific work. A special thanks goes to Dr. Per Stenius for pushing me on the path towards photodarkening resistance, and for both his analysis tutoring and crisp criticism. Without naming everyone I thank all the people working in Liekki Oy (now nLIGHT Oy), from operators to directors, for an invigorating working environment that enabled me to write this dissertation.

I'm grateful to Dr. Dahv Kliner and Dr. Jeffrey Koplow for their help with the data analysis and fresh ideas for further experiments. It was an educating experience to write a manuscript with their feedback and inputs. I thank Prof. Seppo Honkanen for keeping up the

spirit during the last year, and Dr. Goëry Genty and Prof. Jari Turunen for their helpful comments on the manuscript.

Last (and certainly not least) I thank my wife Paula, and my boys Tuomas and Topias for daily clearing my mind of work or scientific matters.

Vantaa, November 2008 Joona Koponen

Contents

Preface **1**

Contents **3**

List of Publications **5**

Author's contribution **6**

List of Abbreviations **8**

1 Introduction **9**

2 Rare-earth doped optical fibers **11**
2.1 Characteristics of amplifying optical fibers 12
2.1.1 Numerical aperture and V-number 13
2.1.2 Cross sections 14
2.1.3 Excited state lifetime 15
2.1.4 Inversion 17
2.2 Manufacturing of rare-earth doped fibers 19
2.3 Applications of rare-earth doped fibers 21

3 Photodarkening in ytterbium doped fibers **22**

4 Spectral properties of photodarkening **25**
4.1 Measurement method 25
4.2 Results 26

5 Temporal characteristics of photodarkening **30**
5.1 Measurement method 30
5.2 Data analysis with a stretched exponential function 33

5.3 Data analysis with a bi-exponential function 36

6 Inversion behavior in photodarkening measurements..... 43
6.1 Inversion in core pumped measurements 44

6.2 Inversion in cladding pumped measurements 50

7 Photodarkening in fiber based lasers and amplifiers..... 55
7.1 Radial distribution of photodarkening..... 56

8 Summary..... 64

References..... 67

Attached publications..... 80

List of Publications

This thesis consists of an overview and of the following publications which are referred to in the text by their Roman numerals.

I J. J. Koponen, M. J. Söderlund, H. J. Hoffman, and S. K. T. Tammela, "Measuring photodarkening from single-mode ytterbium doped silica fibers," Opt. Express **14**, 11539-11544, 2006

II J. Koponen, M. Söderlund, H. J. Hoffman, D. Kliner, and J. Koplow, "Photodarkening measurements in Large-Mode-Area Fibers", Proc. SPIE Vol. **6453**, 64531E, Fiber Lasers IV: Technology, Systems, and Applications; Donald J. Harter, Andreas Tünnermann, Jes Broeng, Clifford Headley III; Eds., 2007

III J. Koponen, M. Söderlund, H. J. Hoffman, D.A.V. Kliner, J.P. Koplow, and M. Hotoleanu, "Photodarkening Rate in Yb-doped Silica Fibers," Applied Optics **47**, 1247-1256, 2008

IV J. Koponen, M. Laurila, and M. Hotoleanu, "Inversion behavior in core and cladding pumped Yb-doped fiber photodarkening measurements," Applied Optics **47**, 4522-4528, 2008

V J. Koponen, M. Laurila, and M. Hotoleanu, "Demonstration of spatial photodarkening in Yb doped LMA fiber laser cavity," Electronics Letters **44**, 960-961, 2008

Author's contribution

The results presented in this thesis are a result of teamwork within the product development group at Liekki Oy during the years 2005-2008. The author has prepared all the publications.

For publication I, the author took part in designing the experiment, and built the experimental setup. The author conducted the principal measurements, and documented and taught the method to others in order to measure a larger volume of samples. The author also participated in the data analysis.

For publications II and III, the author was the principal designer for the cladding pumping experiment, conducted all simulations, built the experimental setups, did the measurements, and participated in the data analysis. The core pumping experiment was as described in publication I.

For publication IV, the author did all the simulations, conducted all the core pumping experiments, and supervised the cladding pumping experiments. The experimental setups used were the result of publications I-III.

For publication V, the author took part in designing the experiment, conducted the simulations, supervised the measurements, and participated in the data analysis.

The results in this thesis have also been presented in several international conferences as post-deadline, invited, and contributed presentations.

List of Abbreviations

ALD	Atomic Layer Deposition
ASE	Amplified spontaneous emission
CW	Continuous wave
DC	Double clad
DND	Direct Nanoparticle Deposition
EDFA	Erbium doped fiber amplifier
HeNe	Helium Neon
IR	Infrared
LMA	Large-mode-area
MCVD	Modified Chemical Vapor Deposition
MMC	Multimode coupler
MM(F)	Multimode (fiber)
NA	Numerical aperture
ODC	Oxygen deficiency center
OVD	Outside Vapor Deposition
PCE	Power conversion efficiency
PD	Photodarkening
RE	Rare earth
SM(F)	Single-mode (fiber)
WDM	Wavelength division multiplexer
WLS	White light source

1 Introduction

Yb doped fiber lasers and amplifiers are an interesting and viable choice for many applications ranging from materials processing to wavelength conversion. Many sources with 1.0-1.1 µm wavelength range are commercially available, such as kW continuous wave (CW) sources [1,2], lower power CW lasers [3], ns regime pulse width sources [4,5], and shorter pulse width sources from ps down to fs regime [6,7]. Further applications can be covered with wavelength conversion for example to green or UV [8-10]. Such devices, particularly devices using fibers with double cladding (DC) structures, have shown increasing peak and average powers, and the limitations of fiber based systems are continuously pushed forward [11,12].

The reliability of Yb fiber laser systems is a sum of many variables, and this thesis focuses on a specific detrimental phenomenon, namely photodarkening (PD), that may affect the Yb doped core of the fiber laser or amplifier. In particular this thesis focuses on the methodology of measuring and benchmarking PD from fibers of different geometries. The goal of PD studies is to increase the PD resistance of the doped fibers, and for this purpose a repeatable method to compare different fibers of varying compositions is required. The principal goal of this work was to develop a method for characterizing the PD propensity of fiber samples, and to obtain the results fast. The study of the driving mechanism behind PD became a subsequent goal

of this work in order to further understand the implications of the PD under different applications.

Since the work on this thesis was begun, knowledge on PD of Yb doped fibers has increased significantly. Prior to the early work described in this dissertation PD of Yb doped fibers was not widely acknowledged as a potential problem, and no reports existed on the spectral and temporal behavior of Yb doped fibers, with the exception of the observed unsaturable absorption in Yb doped fibers induced by the pump wavelength by Paschotta *et al.* in 1997 [13]. The systematic documented work on PD of Yb doped fibers was started in as late as 2005 [14], and during the writing of this dissertation multiple groups are actively studying the PD mechanism, as discussed later.

This dissertation begins with an introduction to rare-earth (RE) doped optical fibers under section 2, and continues with a review of the on-going discussion on the mechanisms of PD in Yb doped fibers under section 3. The further sections describe the results and methodology of this dissertation, with section 4 describing the spectral properties of PD, section 5 describing the temporal characteristics of PD, and section 6 describing the inversion behavior in core and cladding pumping measurements, information on which the prior investigations were based upon. Finally, in section 7, the implications of PD to different fiber laser or amplifier applications is discussed, followed with the summary in section 8.

2 Rare-earth doped optical fibers

Optical fibers made from glass for transmission of telecommunication signals were first experimented in the 1960's, and within just a more than a decade the first low loss (0.47 dB/km) optical fiber was realized in the laboratories of NTT and Fujikura Cable [15]. During the same time first demonstrations of RE doping to silica fiber were done, as the first Nd^{3+} silica fiber amplifier was demonstrated already in 1964 [16], followed soon by the first silica fiber laser doped with Er^{3+}-Yb^{3+} in 1965 [17]. The first major application for the rare-earth doped optical fibers, erbium doped fiber amplifier (EDFA), emerged when optical fibers were already used for telecommunications, and a method to increase the transmission distance was required. The chemical vapor deposition process used for the low loss silica optical fiber manufacturing was modified to enable doping of RE ions to low transmission loss glass [18,19], and quite soon research groups at the University of Southampton and the AT&T Bell Laboratories developed, practically at the same time, the first EDFAs [20,21]. From EDFAs the use of optical fibers as amplifying media have broadened to medical, defense, and industrial applications, with optical output powers extending from the mW telecommunications range to the multiple tens of kW range for materials processing [1].

2.1 Characteristics of amplifying optical fibers

Silica optical fibers typically consist of a doped glass core, a silica cladding, and a second (outer) cladding surrounding the silica cladding. The glass core has the highest refractive index in order to enable single- or multimode light propagation, while the cladding refractive index is lower. In double clad (DC) fibers the outer cladding has the lowest refractive index in order to propagate high numerical aperture (NA) pump light in the cladding, subsequently absorbing the pump light to the core doped with the active rare-earth. The cladding cross section of a doped fiber is typically non-round, as shown in Fig. 2.1, to enhance cladding propagating pump light absorption to the core [22-24].

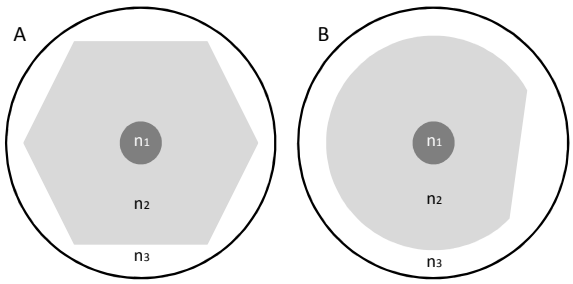

Figure 2.1. Cross section examples of two amplifying optical fibers. A) Hexagonal cladding shape. B) D-shaped cladding. Core has the highest refractive index n_1, cladding has the second highest refractive index n_2 (typically silica), and outer cladding has the lowest refractive index n_3. Core of an amplifying fiber is typically doped with some rare-earth ion(s) and solubility enhancing co-dopants such as Al, or P, or Ge [25-28].

2.1.1 Numerical aperture and V-number

The core refractive index n_1 and the cladding refractive index n_2 define the acceptance angle or the numerical aperture (NA) of the fiber. The core refractive index difference dn is $n_1 - n_2$. The NA of the core (and more generally of a fiber waveguide) can be calculated from the index difference [29]:

$$NA = \sqrt{n_1^2 - n_2^2} \approx \sqrt{2n_1 dn}, \tag{2.1}$$

for instances where $dn << n_1$, which is typical for weakly guided optical fibers [30]. The cladding NA can be derived using the same principle by using the cladding refractive index n_2 and the outer cladding refractive n_3, respectively.

The numerical aperture can be used to define the normalized frequency or V number of a waveguide [30]:

$$V = \frac{2\pi}{\lambda} aNA, \tag{2.2}$$

where a is the core radius of the fiber, and λ is the wavelength in vacuum. The cut-off for single-mode radiation is at $V=2.405$, meaning that at higher V number the fiber is multimoded, whereas at smaller V numbers the fiber is single-moded. Typical single-mode fibers exhibit a

V of 1.8 to 2.4 at the designed wavelength [31]. The large-mode-area fibers used in many amplifying fibers are few- or multimoded, and have larger V numbers. For example the 30 µm core fiber with an NA of 0.07 used in Publication V yields a V number of 6.2 at the wavelength of 1.064 µm.

2.1.2 Cross sections

Cross sections define the radiation emission and absorption probabilities of ions and atoms, and are used in the modeling of rare-earth doped fibers. For a given incoming light intensity I at a predetermined wavelength the absorption and emission cross sections (σ_a and σ_e, respectively) define the absorbed power P_{abs} and the emitted power P_{em}:

$$P_{abs} = \sigma_a I \,, \tag{2.3}$$

$$P_{em} = \sigma_e I \,. \tag{2.4}$$

Cross sections can be estimated using Einstein's A and B coefficients for stimulated emission and absorption, and spontaneous emission. The results given by this approach are, however, typically inaccurate, resulting in errors of at least 25% when calculating the emission cross sections from the measured absorption cross sections [32]. A more accurate method of estimating or calculating the cross sections was

derived by McCumber [33]. McCumber assumed that each Stark level manifold occupation follows the Bose-Einstein-Planck distribution. By also assuming that the time required to establish a thermal distribution within each manifold is short compared to the lifetime of said manifold, the frequency v dependent emission and absorption cross sections are related by

$$\sigma_e(\nu) = \sigma_a(\nu)\exp\left[(\varepsilon - h\nu)/kT\right], \tag{2.5}$$

where k is the Bolzmann constant, T is the absolute temperature, ε is the temperature-dependent excitation energy (i.e. the mean transition energy between the manifolds), and h is the Planck constant. The above equation implies that the emission and absorption cross sections have the same value at only one frequency. Consequently, at lower wavelengths the absorption cross section is always higher than the emission cross section, and at wavelengths above the crossing point the emission cross section is higher than the absorption cross section.

2.1.3 Excited state lifetime

Excited ions mainly decay to a lower energy state either by a phonon (nonradiative) process or a photon (radiative) process [34]. The total excited state lifetime τ of the ion can be expressed

$$\frac{1}{\tau} = \frac{1}{\tau_{nr}} + \frac{1}{\tau_r}, \tag{2.6}$$

where τ_{nr} is the nonradiative lifetime and τ_r is the radiative lifetime. The radiative lifetime is derived from the fluorescence decay of the ion from an energy level to all the energy levels below. The nonradiative lifetime describes the phonon assisted transitions from the excited state to lower energy levels. The nonradiative lifetime is dependent on the number of phonons required to bridge the gap from the excited energy level to the nearest below energy level [35]. The higher the number of phonons required, the less probable the transition becomes. The glass (or crystal) host also influences the number of phonons required, as the phonon energies are host dependent. In silica glasses dopants such as for example aluminum or phosphorus can be used to modify the phonon energies of the host [36-38].

The radiative lifetime can also be calculated, if the emission cross section is known. The equation was derived by McCumber, and yields a radiative lifetime of [33]

$$\frac{1}{\tau_r} = \frac{8\pi n^2}{c^2} \int \nu^2 \sigma_{em}(\nu) d\nu, \tag{2.7}$$

where n is the refractive index of the material, and c is the velocity of light in vacuum.

2.1.4 Inversion

To define inversion we consider a population of ions that can populate three energy levels, see Fig. 2.2. The transition from level 1 to 3 corresponds to the wavelength or energy of the incident pump light flux φ_p, with an absorption cross section of σ_p. The transition from level 3 to 2 is assumed to be nonradiative, and to have a transition rate of $\Gamma_{32}=1/\tau_{32}$, where τ_{32} is the lifetime of the transition. The stimulated transition from level 2 to level 1 is radiative, and corresponds to the wavelength or energy of the signal light flux φ_s with an emission cross section of σ_p. The transition rate of said emission is shown as $\Gamma_{21}=1/\tau_{21}$, where τ_{21} is the lifetime of the transition. The population of each level is given by N_1, N_2, and N_3.

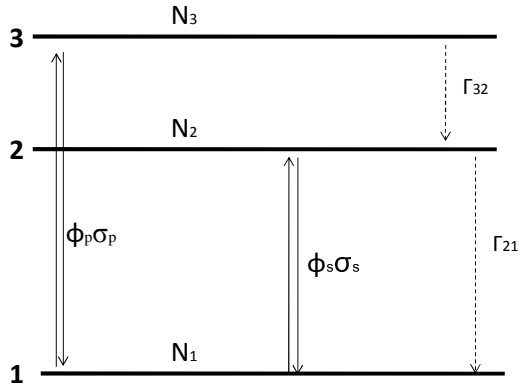

Figure 2.2. Three energy level system. Stimulated absorption and emission shown with line arrows. Spontaneous decay (radiative and nonradiative) shown with dashed arrows.

In simplified models like this the population inversion is typically defined as a state, in which the majority of the ion population is in the excited state, i.e. higher energy level, enabling amplification of the signal radiation. The rate equations of the population changes can be written using the above definitions [34]:

$$\frac{dN_3}{dt} = -\Gamma_{32}N_3 + (N_1 - N_3)\phi_p\sigma_p, \tag{2.8}$$

$$\frac{dN_2}{dt} = -\Gamma_{21}N_2 + \Gamma_{32}N_3 + (N_2 - N_1)\phi_s\sigma_s, \tag{2.9}$$

$$\frac{dN_1}{dt} = \Gamma_{21}N_2 - (N_1 - N_3)\phi_p\sigma_p + (N_2 - N_1)\phi_s\sigma_s. \tag{2.10}$$

The total population N is simply

$$N = N_1 + N_2 + N_3. \tag{2.11}$$

In a steady state situation all the time derivatives will be zero (and thus equal). In typical lasing media the transition rate from level 3 to level 2 can be assumed to be high, in practice reducing N_3 to zero. With these assumptions one can derive from Equations 2.8-2.11 the population inversion N_2-N_1:

$$N_2 - N_1 = \frac{\phi_p \sigma_p - \Gamma_{21}}{\Gamma_{21} + 2\phi_s \sigma_s + \phi_p \sigma_p} N, \quad , \tag{2.12}$$

which subsequently becomes inversion fraction when divided with N.

The model used in the Liekki Application Designer (and thus in the results of Publications II-V) takes into account the different values of absorption and emission cross sections for each wavelength. Due to the differences in the emission and absorption cross sections gain can be achieved with less than half of the ions in the excited state. Liekki Application Designer defines the inversion as the fraction of ions in the upper energy level, i.e. N_2/N.

2.2 Manufacturing of rare-earth doped fibers

The general process for manufacturing a rare-earth doped fiber consists of manufacturing the core, refining the core into a preform, and drawing the preform to a fiber [34].

Rare-earth doped core can be manufactured using various methods, for example with modified chemical vapour deposition (MCVD) and solution doping, outside vapor deposition (OVD), direct nanoparticle deposition (DND), or MCVD and atomic layer deposition (ALD) [39-43]. All methods have in common that first small, sub-millimeter silica particles (called soot) are generated, either by

hydrolysis (for example OVD) or oxidation (for example MCVD, DND) of precursors. Silica soot is either formed with the required dopants, or the dopants are added to the soot in a subsequent process step such as solution doping or ALD. Soot can be further treated for example in increased temperature and controlled atmosphere to reduce impurities and water [34]. The dehydration is often required, as most rare-earth chlorides (typically used as precursors) are hydrated. Silica soot is then sintered to glass, i.e. raised to a temperature where the small silica particles are bonded together by solid-state diffusion [44], and collapsed into a rod. The preform has the same core/cladding ratio and geometry as the fiber. Due to this the rod can then be sleeved with one or multiple glass tubes to form the preform.

The last step in fiber manufacturing is the fiber drawing. The preform is placed vertically into an oven at the top of a fiber draw tower. Typical oven temperature range for silica fiber drawing is 1950-2200 ºC [45]. The preform is heated from one end until the glass melts, and the preform starts elongating rapidly due to gravity. By starting with the elongated end the fiber is then pulled to its designed diameter using rollers at the bottom of the tower. The height of the drawing tower enables the fiber to cool down and be coated with a polymer prior to the spooling at the bottom of the tower. The diameter of the fiber can be optically measured during the draw, and the fiber diameter can be controlled by varying the preform feeding rate, oven temperature, and pull velocity.

2.3 Applications of rare-earth doped fibers

Rare-earth doped fibers are used typically as amplifiers or lasers. As discussed earlier, EDFA was the breakthrough application for doped active fibers. EDFAs are typically core pumped, i.e. the pump light is coupled to the rare-earth fiber as single-mode radiation propagating in the core of the fiber [21,20]. With core pumping the output power of the system is limited by the availability of single-mode pump sources. Alternative method of coupling the pump power to the doped fiber is by using double clad fiber, in which multimode pump light can propagate in both the core and the cladding parts of the fiber, enabling higher pump power. Power scaling of the rare-earth fibers started with the diode cladding pumping of a fiber with a Nd^{3+} doped core [46]. As diode brightness and efficiency have increased, the brightness and output powers of fiber lasers and amplifiers have increased as well. For high power applications the Yb^{3+} fibers have been particularly interesting due to the high efficiency that is primarily due to the low quantum defect when pumped near the 976 nm absorption peak [47]. The applications of the rare-earth doped lasers and amplifiers range from telecommunications to materials processing and wavelength conversion [1-7].

3 Photodarkening in ytterbium doped fibers

PD manifests as a gradually increasing spectrally broad transmission loss in the Yb doped core of a fiber. PD can be attributed to the formation of color centers or other light-induced structural deformations in the doped glass core [48]. While most of the excess loss is induced at visible wavelengths, a significant amount of PD may also be present at the near-infrared (IR) signal and pump wavelengths. The PD process is driven largely by the energy of signal and pump photons causing optical losses in the doped core only; the process is thus distinguishable from other detrimental effects, such as polymer coating damage (causing cladding propagating pump light losses) or glass radiation damage from high-energy particles (forming without interaction with signal or pump photons).

Typically, high-power fiber devices are realized with DC, large-mode-area (LMA) fibers (i.e., large core diameter and low numerical aperture, NA). The relatively long application lengths of DC fibers, particularly when compared to bulk crystals, are beneficial in spreading the induced heat load over a larger area to volume ratio [49]. LMA fibers are of interest because the resultant decrease in irradiance at a given power level (or decrease in fluence at a given pulse energy) mitigates optical damage and increases the threshold for undesirable nonlinear processes. In addition, the length of the doped LMA fiber

may be shortened by increasing the core/cladding area ratio and/or by increasing the Yb concentration, resulting in higher pump absorption. For many applications, shortening the length of the Yb-doped fiber is highly beneficial, for example, in reducing nonlinearities in high-peak-power amplifiers [50]. On the other hand, higher concentrations and/or higher pumping rates have been associated with deleterious effects, the most troublesome of which is the phenomenon of PD, generally acknowledged as a process that can potentially limit both the efficiency and lifetime of Yb-doped fiber devices. Reduction, or preferably elimination, of this damage mechanism would greatly enhance the prospects for development and fielding of practical fiber lasers and amplifiers in applications requiring predictable performance in long-term operational settings. To achieve this goal, meaningful characterization tools, as well as better understanding of the PD phenomenon, must be developed.

Photodarkening of rare-earth doped fibers has been reported for many different glasses doped with, for example, Tm^{3+}, Ce^{3+}, Pr^{3+}, Eu^{2+}, $Tb^{3+}$and Yb^{3+} [13,51-55]. The PD was typically attributed to a multistep multiphoton absorption process, wherein a single RE ion is excited to a high energy state, and a UV photon is likely emitted and subsequently absorbed, forming a color center via a glass ionization process. In the case of Yb, the mechanism behind PD remains largely unexplained, and several possibilities have been presented. Yoo *et al.* [56] used a CW 488 nm light source to induce excess loss in doped

aluminosilicate fibers and observed a spectroscopic peak at 220 nm, which was attributed to Yb-associated oxygen deficiency centers (ODC). Based on comparisons with measurements on Yb-free fiber samples, it was suggested that these centers could act as precursors of PD in Yb-doped aluminosilicate fibers. Engholm et al. presented results supporting the formation of Yb^{2+} ions in the glass matrix from Yb^{3+} through a charge transfer process, resulting in free holes that can act as precursors for color centers [57]. A similar observation was reported earlier by Guzman Chávez *et al.* [58], who suggested the potential formation of Yb^{2+} in a process involving interaction of Yb^{3+}-Yb^{3+} pairs or even more complicated ion clusters. There have also been indications that fibers with lower Al and/or higher Yb concentrations exhibited increased PD [59,60], whereas Yb-doped phosphosilicate fibers, which are known to provide high solubility to Yb ions and thus exhibit less clustering, showed greater PD resistance [61]. Previous work has also shown the PD process to be either partially or fully reversible in many cases. Methods used to bleach PD have included temperature annealing [62], exposure to UV and visible light [58,63], and oxygen loading [56]. More recently PD has also been shown to bleach by the pump power itself [64].

4 Spectral properties of photodarkening

Photodarkening in Yb doped fibers has characteristic properties in both spectral and temporal domain. The spectral properties may give indications to the underlying physical phenomena, and can be used for example in comparing and benchmarking fibers for PD. The spectral properties of PD were studied mainly in publication I, and some of the findings were originally presented in a conference [14].

4.1 Measurement method

Measurements of the PD spectra were studied using a measurement setup illustrated in Fig. 4.1. A typical measurement consisted of first measuring the transmission of the fiber sample using the white light source and the spectrum analyzer, after which the single-mode fiber coupled pump diode was used to photodarken the Yb doped fiber sample. The transmission of the photodarkened sample was measured, and the induced excess loss spectra was calculated by taking into account the sample length. The inversion level of the fiber was repeatable between samples due to inversion saturation, as described later under section 6.

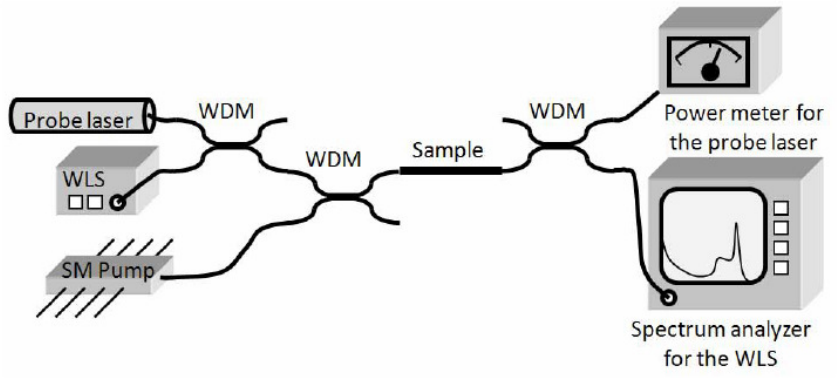

Figure 4.1. Measurement setup for PD characterization. The white light source (WLS) can be used to measure the fiber sample prior and after PD. PD is induced by illuminating the sample with a single-mode pump diode. Probe laser can be used to measure in real time the increased loss at the probe laser wavelength. Wavelength division multiplexers (WDM) can be used to separate and combine different wavelengths.

4.2 Results

Two typical excess loss spectra after 30 minutes of pump illumination are shown in Fig. 4.2. Highest loss is induced at visible wavelengths, but the absorption tail reaches to the IR region of interest in Yb doped fiber applications. Spectral shape of the induced loss at visible and IR was later studied by multiple groups, and the results are mainly in agreement with the presented work [58,62-65].

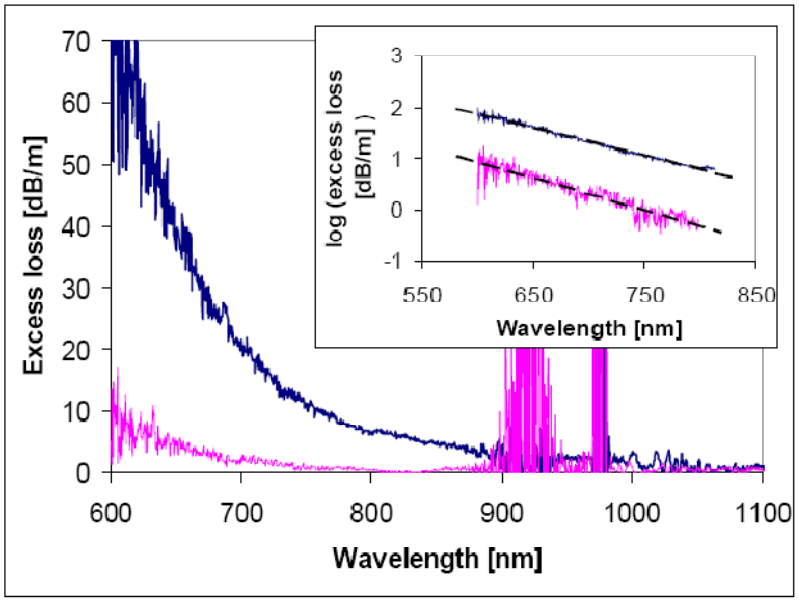

Figure 4.2. Typical PD induced excess loss spectra ranging from visible to IR. The two curves represent two different measurement points of fibers with dissimilar Yb ion concentration. Data in the 900-1000nm window was below the detector noise floor.

As seen from the typical measurement data the shape of the induced loss between the fibers is similar. It is also evident that the signal to noise ratio of the spectral loss is higher at the visible wavelengths than at the 1 µm wavelength range, that is of interest to Yb fiber applications. Assuming the spectral shape between samples is similar, the induced loss at signal wavelength should correlate to the loss at shorter wavelengths. This was studied by measuring 22 different Yb doped aluminosilicate glass compositions, with approximately two measurements per composition. The wavelength of 633 nm was chosen

to be the reference wavelength due to the possibility of later using a HeNe laser probe laser in temporal measurements. Results of the test series are shown in Fig. 4.3. The PD induced excess loss had a clear correlation between the wavelengths of 633nm and the average over 1040-1070nm, and the slope averaged over the test data suggests an approximately 71 times higher induced loss at 633 nm than at the signal wavelength.

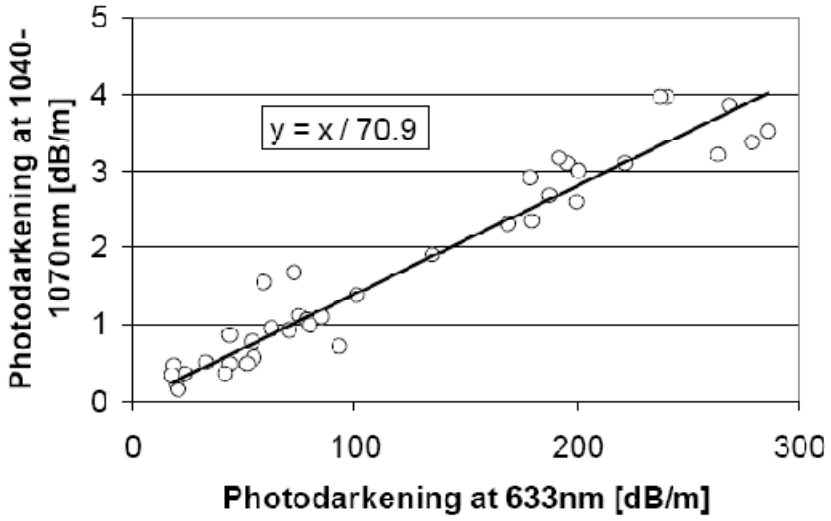

Figure 4.3. PD induced losses at wavelengths of 633 nm and the signal wavelength 1040-1070 nm.

The spectral shape of PD induced loss is derived from multiple factors: the types of color center(s) formed (spectral shape, absorption cross section), and the fractions of different loss sites in the glass. If there were multiple types of color centers in the glass, the formation

kinetics and the time and inversion used to induce the PD loss would play a role in defining the fraction of different sites. Although the spectral shape was relatively constant within the presented data it is likely that glasses with vastly different constituents (for example using co-dopants such as Ge, P, or Al) and structure would exhibit a different spectral response in a PD measurement, as the data in [65] suggests.

5 Temporal characteristics of photodarkening

The temporal dynamics of PD in Yb doped fibers were the main theme of publications II and III. The key hypothesis was that the rate of PD is driven by the inversion level of the fiber sample. The hypothesis was based on the observation that by fully inverting the fiber under test the rate of PD was no longer dependent on the pump intensity [66], which one would not expect from for example a multi-photon absorption process similar to the observed PD of Tm^{3+} or Tb^{3+} [52,53]. By studying the evolution of the induced loss as functions of time and inversion some further knowledge of the physical process underlying the PD phenomena can be uncovered, and conclusions can be drawn for the implications of the PD process to different fiber applications.

5.1 Measurement method

The PD rate results shown in this thesis were measured using the cladding pumping method shown in Fig. 5.1. The measurements were conducted by using a core coupled 633 nm HeNe probe laser, and by measuring the transmission change of the probe laser during the exposure of the fiber sample to cladding propagating pump light. The cladding propagating signal and pump light were stripped using a single-clad single-mode fiber. Further spectral filtering was used to

separate the core propagating pump and probe beams. The analysis of the results required obtaining the inversion value of the fiber sample. The inversion levels of the fiber samples were simulated, following the methodology described under section 6 Inversion behavior in photodarkening measurements. The probe laser wavelength was chosen in order to be able to correlate measured losses to the signal wavelengths as demonstrated under section 4.

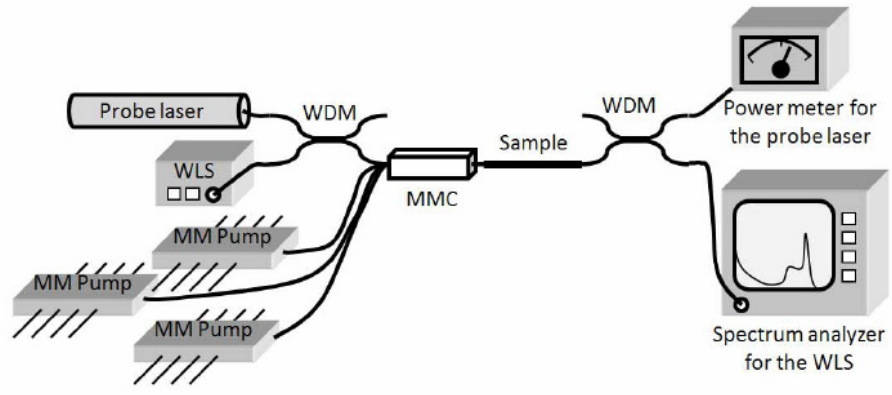

Figure 5.1. Cladding pumping method used to measure PD rate in Yb doped fiber samples. Multimode pumps are coupled via the multimode coupler (MMC) used to induce inversion in the sample, and the transmission through the core can be measured with a WLS or a probe laser by using a spectrum analyzer or a power meter, respectively.

The initial finding of the measurements was that the rate of PD is strongly dependent on the inversion of the fiber sample, as shown in Fig 5.2. In fact, the results of the measurements showed a higher

inversion to rate dependency than what was anticipated. Due to this, care was taken to remove or identify possible error sources such as temperature effects or probe laser / detector drift by for example cooling the fiber sample. The measurement results were observed not to follow an exponential decay rate, which was expected based on the existing literature on PD observed in glasses doped with other RE ions [51,53]. The first analysis of the results presented here were conducted using a stretched exponential function [67], as described in detail under section 5.2. As the stretched exponential function is typically described to be an exponential function with a temporally varying decay rate, it is difficult or impossible to get a meaningful physical explanation for the observed behavior. To overcome this shortcoming a more thorough study of the results was conducted using a bi-exponential function for curve fitting as described under section 5.3, that yields two exponential functions of different amplitude and fraction for the PD rate.

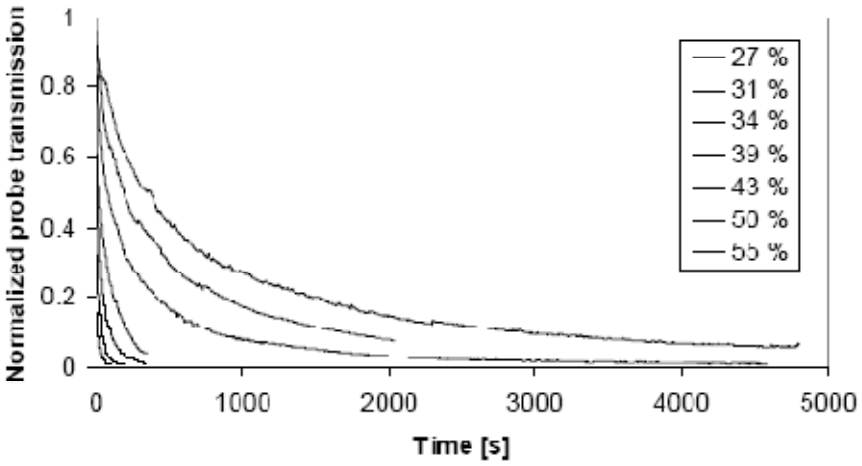

Figure 5.2. Measured 633 nm probe transmission through a single-mode fiber sample while cladding pumped to varying inversion levels (from 27% to 55% in the top to bottom order).

5.2 Data analysis with a stretched exponential function

The PD transmission data from two different fibers and with several induced inversion levels were measured using the setup described in Fig. 5.1. For each transmission measurement, the normalized, time-dependent probe transmission (T) was fitted with a stretched exponential function [67]

$$T(t) = A\exp\left[-\left(\frac{t}{\tau}\right)^{\beta}\right] + (1-A), \tag{5.1}$$

where (1-A) is the steady state transmission, β is the stretch parameter ($0 \leq \beta \leq 1$), t is time, and τ is the PD time constant for each measurement. The fitting was done using the least-squares method, and the parameters that gave the best agreement with the measured data were β = 0.675, and A = 0.99 for Fiber #1 and β = 0.65 and A = 0.98 for Fiber #2. Using the same fitting values for both fibers does not significantly influence the results. The best-fit parameters above were used for all data handling of the corresponding fiber results in the data analysis.

Figure 5.3 shows a log-log plot of the inverse of the PD time constant as a function of the inversion level. The linearity of the data points suggests that the initial PD rate (the inverse of the PD time constant) is an exponential function of inversion (I), namely

$$\frac{1}{\tau} \propto I^{n} \Rightarrow \log\left(\frac{1}{\tau}\right) \propto n\log(I). \tag{5.2}$$

The slope n of the linear fit is approximately 7 for both fibers, i.e., based on the results, the initial PD rate has a seventh-order dependence of the inversion level.

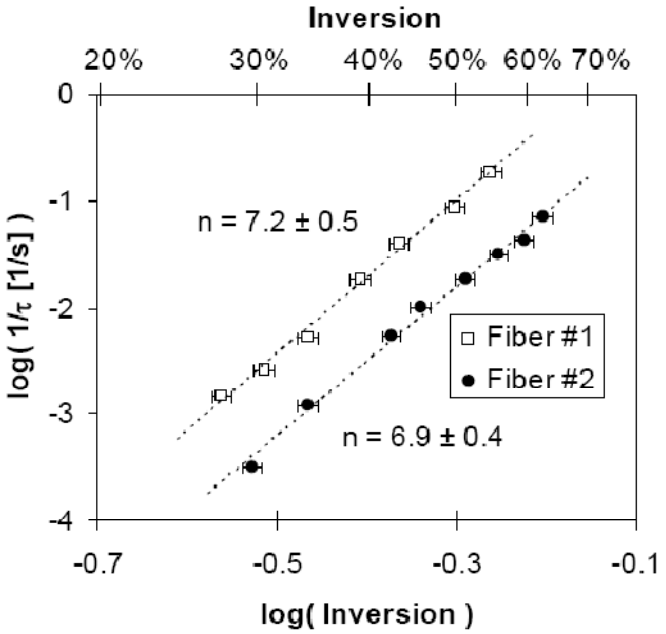

Figure 5.3. Stretched exponential time constants of two different fiber samples as a function of inversion. Both measurements show a slope of approximately seven.

The fiber samples were of similar aluminosilicate glass composition, however, they had different Yb concentrations. The data shown in Fig. 5.3 can be re-plotted as a function of the Yb excited-state number density [Yb*], which is the inversion multiplied by the Yb concentration, as shown in Fig. 5.4. Plotted in this manner, the results for the two fibers are identical within experimental error. This result shows that, for the glass composition of these fibers, the initial PD rate

is determined exclusively by the number density of excited Yb ions, not by Yb concentration or pump level, with a seventh-order dependence on [Yb*].

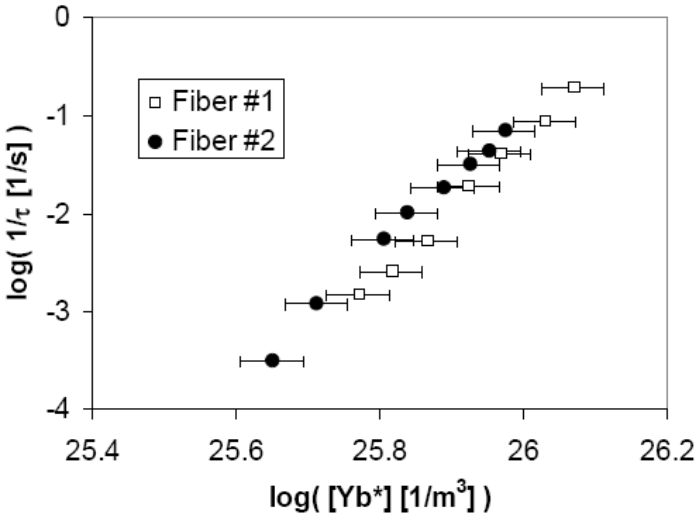

Figure 5.4. Stretched exponential time constants of the two fiber samples as a function of excited ion number density.

5.3 Data analysis with a bi-exponential function

The measurement data used under section 5.2 was analyzed further using a bi-exponential function. The analysis was based on the measured transmittance and its relationship to the concentration of color centers formed by the PD process. The transmitted probe-laser intensity (I) is given by Beer's Law:

$$I = I_i e^{-\sigma NL}, \tag{5.3}$$

where I_i is the incident intensity, σ is the absorption cross section of the color center (at the probe wavelength), N is the concentration of color centers, and L is the sample length. The concentration of color centers is known to vary with time and is presumed to reach a final concentration level (N_f).

Consider now a mechanism that exhibits a multi-exponential time dependence (i.e., multiple time constants) for n pathways. The time-dependent concentration of color centers is then given by:

$$N(t) = N_f (1 - \sum_{i=1}^{n} c_i e^{-t/\tau_i}), \tag{5.4}$$

where the coefficient c_i is the amplitude of process i with time constant τ_i, and

$$\sum_{i=1}^{n} c_i = 1. \tag{5.5}$$

Equations (5.4) and (5.5) assume that the various pathways lead to the same final state, which is reasonable in light of our previous observation of similar loss spectra in various fibers that have undergone PD, as discussed under section 4.

In general, the signal incident on the detector may include residual pump light propagating in the core (part of which may reach the power meter even after spectral filtering) and probe light propagating in the inner cladding of the fiber (which experiences very little attenuation within the gain fiber before reaching the detector). The following equations take these contributions into account: we define f as the fraction of pump light propagating in the core of the fiber and P as the residual pump light. The measured signal ($I_{norm(t)}$) normalized to the initial signal present on the detector (I_0) is given by:

$$I_{norm}(t) = \frac{I(t)}{I_0} = \frac{I_i f e^{-\sigma N(t) L}}{I_i + P} + \frac{(1-f) I_i + P}{I_i + P}. \tag{5.6}$$

Consider the case of two first-order processes [n = 2 in Eq. (5.4)]. By expanding Eqs. (5.4) and (5.6) and grouping parameters, the normalized intensity following the bi-exponential growth of N(t) is given by:

$$I_{norm}(t) = C_1 (e^{-C_2 (1 - C_3 e^{-C_4 t} - (1 - C_3) e^{-C_5 t})} - 1) + 1, \tag{5.7}$$

where

$$
\begin{aligned}
C_1 &= \frac{I_i f}{I_i + P}, \\
C_2 &= \sigma N_f L, \\
C_3 &= c_{1,} \\
C_4 &= 1/\tau_1, \\
C_5 &= 1/\tau_2.
\end{aligned}
\tag{5.8}
$$

Equation (5.7) has 5 adjustable parameters, and obtaining a good fit to the data would not be strong evidence that this equation is uniquely suited to describing the PD process. We can use physical arguments, however, to constrain many of the parameters. We can first set $C_1 = 1$ assuming that there is no probe light propagating in the cladding, residual pump light, or detector offset: we estimate that such effects contribute at most 10% to the total signal and can thus be neglected at first. Second, C_2 contains constants that should not vary from sample to sample of the same fiber or between fibers of similar composition; thus, C_2 can be assumed constant for a given fiber type and was therefore not varied in fitting the various PD curves recorded at different pump powers. Similarly, C_3 which reflects the relative amplitudes of the two pathways, is also expected to remain constant for a given fiber type. With these assumptions, we are left with just two adjustable parameters; after establishing values for C_2 and C_3, only C_4 and C_5 (i.e., the two first-order rate constants: one fast and one slow) were varied to fit each PD decay curve.

The inversion to PD rate results of both fibers are shown in Fig. 5.5. The data from both fibers had similar constant values ($C_{2,3}$),which was not surprising after the similar constant values obtained from the stretched exponential fitting. The slopes of both fast and slow PD rates were within 7 ± 1, yielding a similar result as obtained from the stretched exponential data analysis, with the exception that the bi-exponential results can be interpreted to be caused by two parallel mechanisms following exponential functions of different amplitude and rate. The relative amplitudes of the two pathways are ~4:1 for both fibers, favoring the slow process, and the rate constants differ by a factor of ~10.

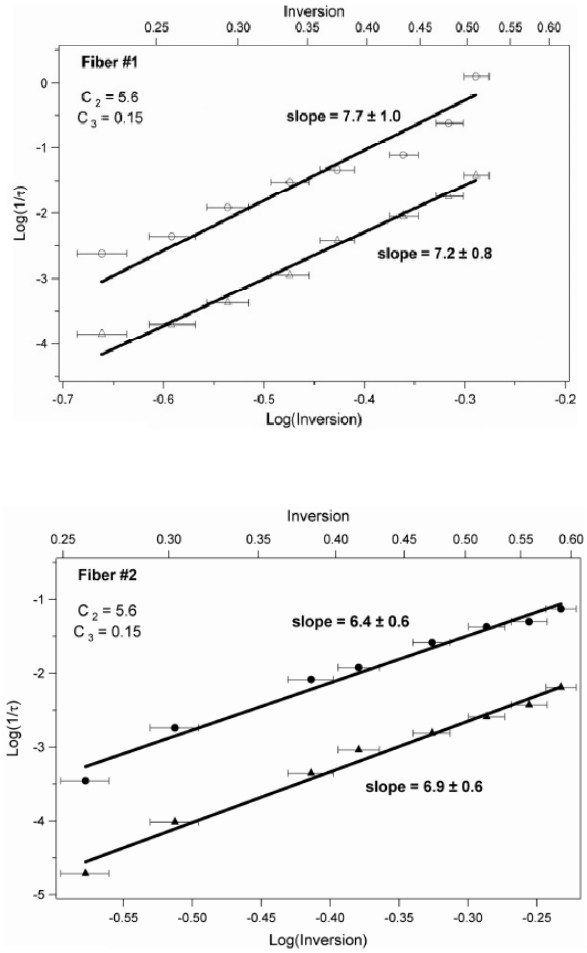

Figure 5.5. Measured fast and slow PD rate constants for fiber #1 (top and fiber #2 (bottom) as a function of inversion. The slope values are within 7±1.

The data shown in Fig. 5.5 was re-plotted taking into account the ion density of each sample. The resulting PD rate correlation with the excited Yb ion density [Yb*] is shown in Fig. 5.6.

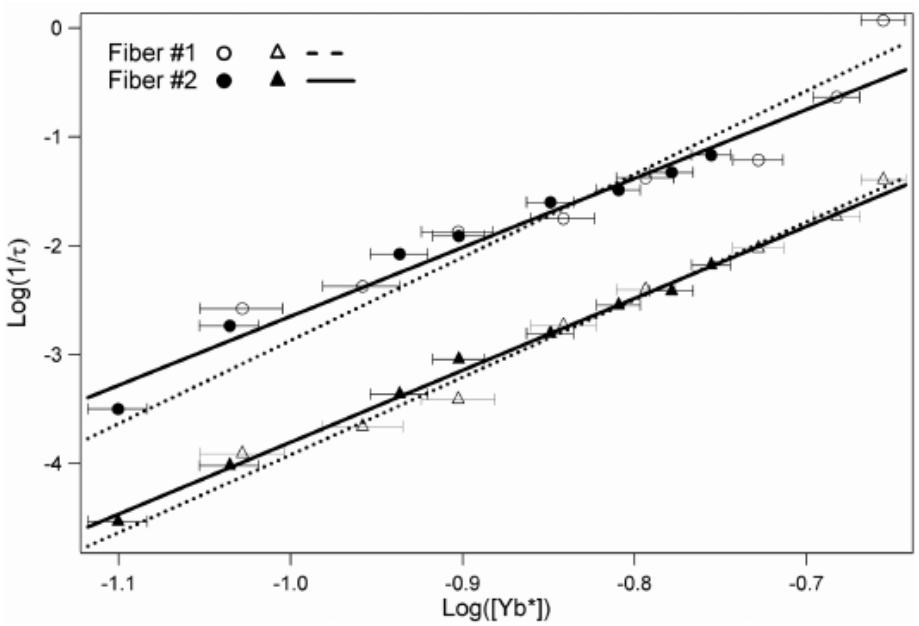

Figure 5.6. Measured fast and slow PD rates for both fiber #1 and fiber #2 as a function of excited Yb ion number density. The slopes correspond to the same slopes as in Fig. 5.5.

The analysis supports the findings of the stretched exponential case, i.e. with similar glass compositions the PD rate is controlled by a single parameter, [Yb*], and the PD time constants followed a simple power law, and were proportional to ~$[Yb^*]^7$.

6 Inversion behavior in photodarkening measurements

In PD measurements the control of inversion in the fiber sample is essential for the interpretation of the results, the reproducibility of the measurements, and the temporal characteristics of the measurement. The inversion behavior in PD measurements was the principal theme of publication IV. Two cases are considered, the core pumping method and the cladding pumping method, illustrated in Figs. 4.1 and 5.1, respectively. The results are based on numerical simulations, and examples of measurement data for specific simulation cases are presented.

All simulations described in this thesis were done using a commercially available fiber simulation tool, Liekki Application Designer v4.0, and the cross section data (shown in Fig. 6.1) based on measurements of aluminosilicate Yb doped fibers conducted at Liekki Oy.

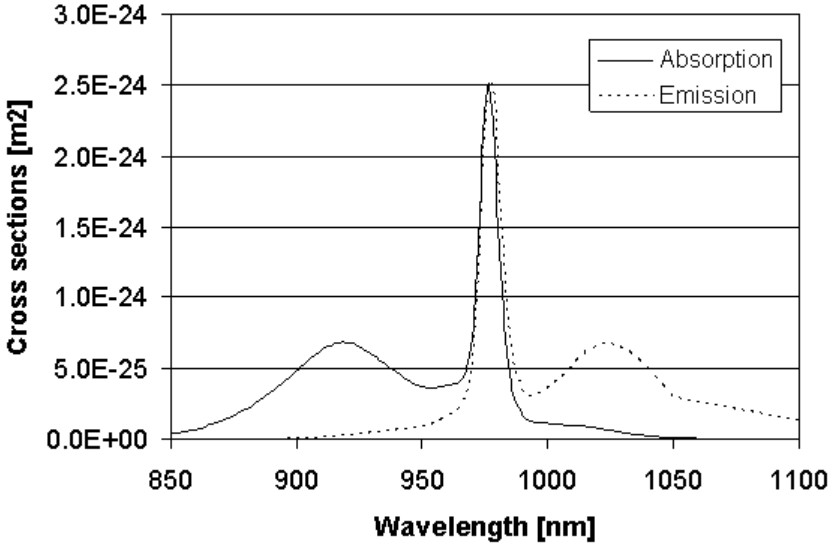

Figure 6.1. Absorption and emission cross section data used to obtain the presented simulation results.

6.1 Inversion in core pumped measurements

The inversion profile of a core-pumped sample was simulated as a function of pump power, sample length, Yb ion concentration, and pump wavelength for a 4 μm core diameter fiber. The average inversion over the whole sample and the standard deviation of the inversion were calculated from the simulated inversion profiles. The inversion data was obtained for each longitudinal simulation point. Each longitudinal inversion point is the average of the radial inversion, and in cases

where the inversion is defined to be flat (i.e. <1% standard deviation over the length of the sample) also the radial inversion profile was confirmed to be flat. Fig. 6.2 illustrates how the inversion of a 10 cm core-pumped sample saturates with increasing pump power at two different pump wavelengths. The inversion level of a fiber changes very little with increased pump power when the inversion is flat. Due to the short sample length and the high brightness of the pump the amplified spontaneous emission (ASE) contribution to the inversion is small.

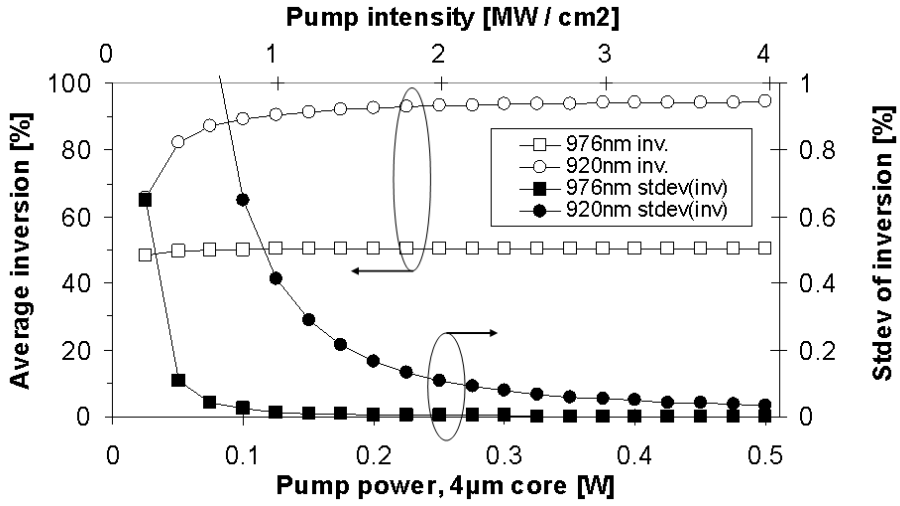

Figure 6.2. Inversion in a core pumped 10 cm sample of 4 µm core diameter fiber.

A general view of the influence of pump wavelength is shown in Fig. 6.3, where each point represents the average inversion of a particular sample length irradiated with 250 mW of pump light. The

saturation level of inversion follows approximately the ratio of the absorption and emission cross sections at the pump wavelength. The longer samples at 920 nm show a decreased average inversion. The pump power used was not high enough to saturate the inversion in those data points, and the inversion profiles of the simulated fiber samples were not flat.

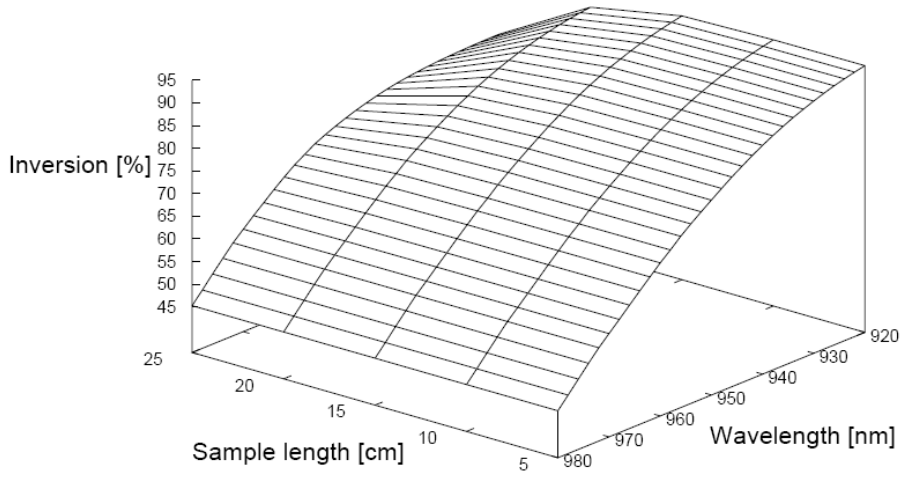

Figure 6.3. Inversion in 4 μm core diameter with varying sample lengths and pump wavelengths.

The scalability of the core pumping method to larger core diameters is shown in Fig. 6.4, where the simulated pump power required for inversion saturation of a 10 cm sample is illustrated for two different pump wavelengths. The simulations were done using the typical parameters listed above. The pump power required to saturate a core pumped sample increases as the core diameter increases, but the

required fluence is constant. This limits the core size of a practical benchmarking measurement to approximately 9 µm (920 nm pump) and 18µm (976 nm pump) with 500 mW of coupled pump power. Practical limitations such as splice losses between dissimilar fibers and the availability of high brightness pumps further limit the core diameters, making the core pumping method suitable mostly to single-mode and few moded fibers up to 10 to 15 µm diameter when using the 976 nm pump wavelength.

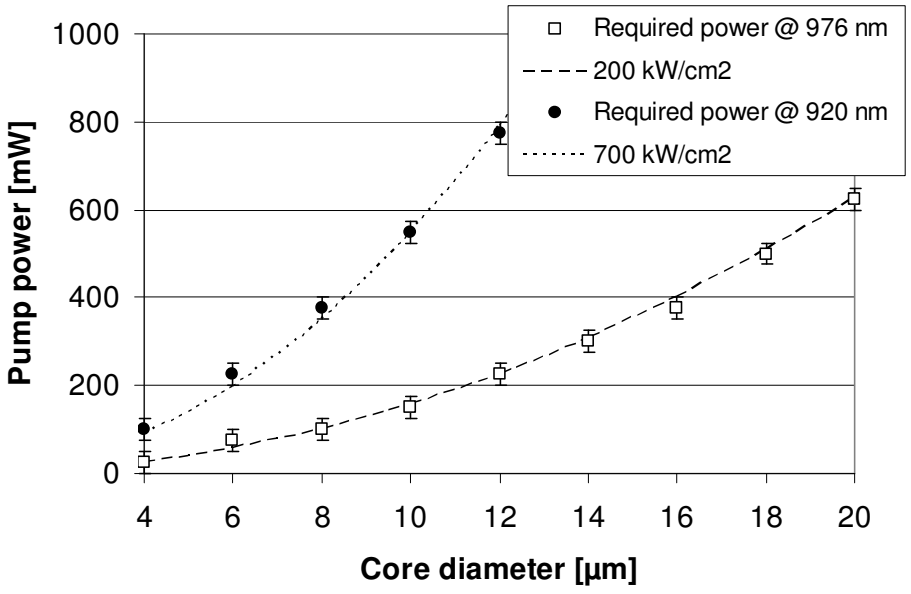

Figure 6.4. Limits of core pumping method. The inversion saturation in the core pumping method is achieved with lower irradiance when pumped close to the pump absorption peak at 976 nm.

To highlight the key properties of the core pumping setup PD experiments were conducted using a setup similar to shown in Fig. 4.1. The measurements were done using a 974 nm fiber coupled pump and a fiber coupled HeNe probe laser operating at 633 nm wavelength. In the first set of experiments, illustrated in Fig. 6.5, the fiber length of each sample was chosen to be 50 cm. The coupled pump power of each sample was different (from 30 to 70 mW), and the simulated inversion profiles are shown in the inset of the figure. The rate and degree of PD differ significantly between the pump powers within the duration of the experiment. This was attributed to the dissimilar inversion profiles of each pumped fiber. As pump power was increased, a longer length of the fiber sample was saturated to the high inversion level of ~50%. In essence, only the sample length that was under high inversion was varied by changing the coupled pump power.

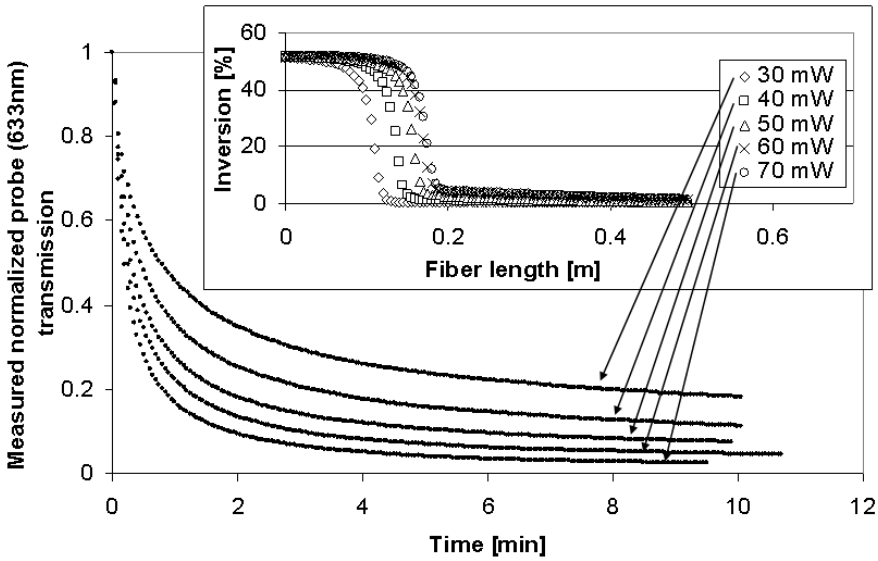

Figure 6.5. Measured normalized probe transmission (HeNe laser at 633 nm) as a function of time for 50 cm fiber samples. Inset: simulated inversion profiles of each sample.

Measurements conducted to the 50 cm samples indicated the importance of a proper sample length when benchmarking or studying fibers using the core pumping method. A second set of measurements was done to shorter samples of 10 cm each. The resulting normalized probe transmissions are illustrated in Fig. 6.6, and the simulated inversion profiles for the fibers are shown in the inset. The principal finding of the data is, that as the inversion profile of the fiber is saturated (inversion profile same for all coupled pump powers) the rate of PD is constant between the samples within experimental error.

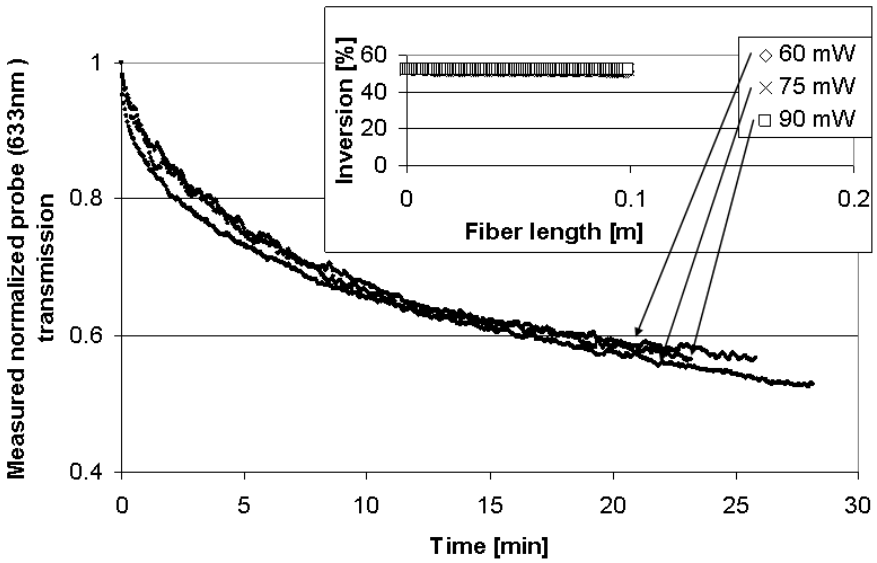

Figure 6.6. Measured normalized probe transmission (HeNe laser operating at 633 nm) as a function of time for 10 cm fiber samples. Inset: simulated inversion profiles are all shown, but overlap.

6.2 Inversion in cladding pumped measurements

As stated earlier the core pumping method can readily be applied only to measurements of fibers of limited core diameter. To readily achieve a flat inversion in fibers with core diameters larger than 10-15 µm, a different approach of inducing the inversion is required. Cladding pumping using multimode pump diodes, as shown in Fig. 5.1, fulfills the requirement. Inversion of a 20 µm core diameter and 400 µm

cladding diameter was simulated with varied pump powers and two different pump wavelengths. The resulting inversions are shown in Fig. 6.7, indicating that a flat inversion is achieved over the whole range of launched pump power. The achieved inversion is however a function of the pump irradiance. A typical operational regime for LMA fibers is far from the intensity thresholds for inversion saturation; 200 kW/cm^2 irradiance in a 400 µm diameter fiber translates to approximately 250 W of pump power, which is feasible but hardly practical for a benchmarking measurement.

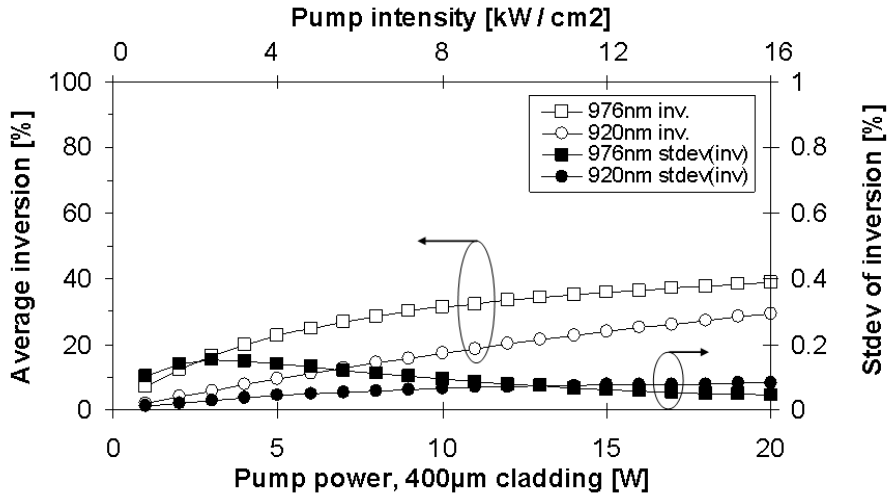

Figure 6.7. Inversion in a cladding pumped 20 µm / 400 µm diameter core / cladding fiber with varying pump powers and two typical pump wavelengths.

The pump wavelength dependence of a low irradiance cladding pumped sample was studied by simulating the inversion profile of a

fiber sample over a range of pump wavelengths and fiber lengths, as shown in Fig. 6.8. The plotted inversion is the average inversion of the fiber sample of a certain length, i.e. the graph does not quantify the flatness of the inversion profiles. However, the inversion in the samples was flat within the shown wavelengths and sample lengths. The coupled pump power was 5 W, and the core and cladding diameters were 20 µm and 400 µm, respectively, for the results shown. Due to the low intensity of the pump light the average inversion is defined mainly by the absorption cross section. In order to induce a comparable inversion between different fiber samples one needs to have a repeatable pump wavelength and coupled pump power to the samples.

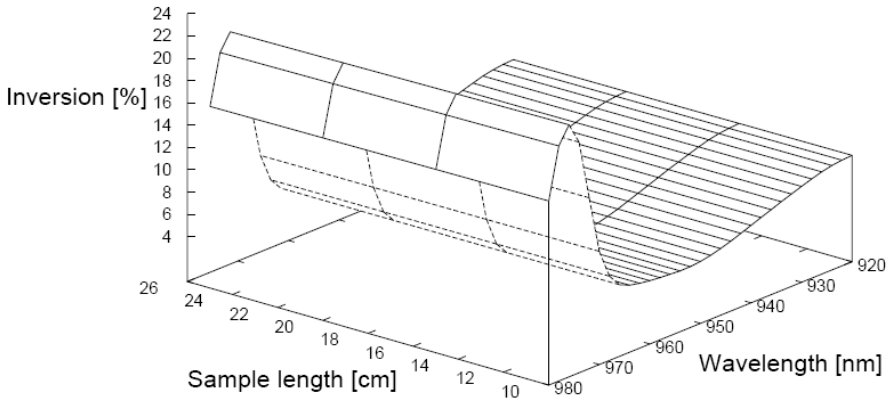

Figure 6.8. Inversion induced by the cladding pumping method with 5 W of coupled pump power and 20 µm / 400 µm diameter core / cladding fiber.

Experiments that describe one of the key properties of the cladding pumping method, inversion to the coupled pump power dependency, were described under section 4. All of the measurements were conducted to samples of the same length, i.e. 10 cm of fiber. As the inversion level of the cladding pumped samples is dependent on the pump irradiance, and the PD rate is sensitive to the achieved inversion fraction, a set of measurements was done to study the effect of the sample length to the measurement. Three different lengths (9.5, 23.5, and 50 cm) were measured, each with two pristine fiber samples of 30/250 µm diameter core/cladding fiber. The results are illustrated in Fig. 6.9, and the simulated inversion profiles are shown as inset. The induced transmission losses (measured at 800 nm) are normalized with the samples lengths in order to obtain comparable data. Two conclusions can be drawn from the data: the length of the sample has a significant impact to the induced PD due to the decreased inversion along the fiber, and to obtain repeatable inversion profiles the sample lengths need to be constrained to lengths that do not induce significant ASE, as is the case in the longest sample with decreased inversion levels at both ends of the sample due to ASE.

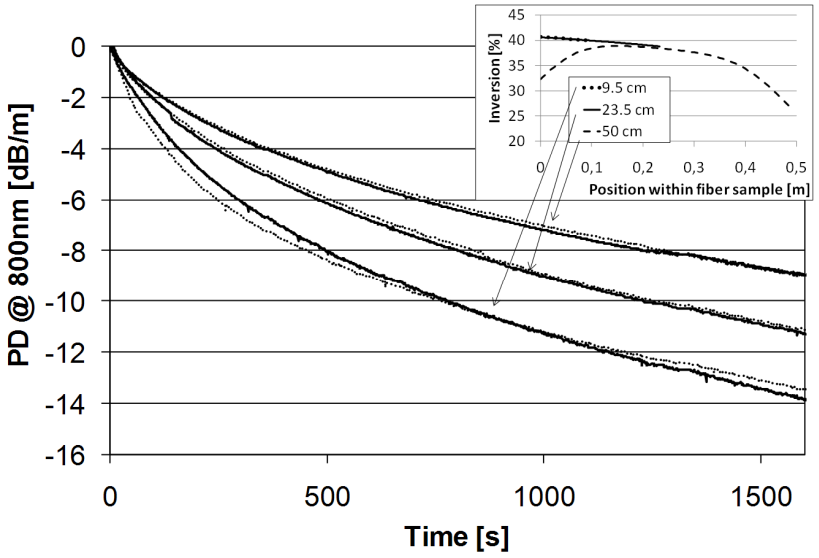

Figure 6.9. Measured transmission of cladding pumped samples of different lengths, normalized with the sample lengths. Inset: simulated inversion profiles of the samples. Each length was measured twice with a pristine fiber sample.

7 Photodarkening in fiber based lasers and amplifiers

From the viewpoint of a fiber laser or amplifier manufacturer the goals for the spectral and the temporal studies of the PD propensity described in the previous chapters are to be able to compare fibers, and to estimate the lifetime of a fiber susceptible to PD in varying operating conditions and applications. The PD rate inversion dependency enables extrapolation of the implications of PD to different applications. Based on the experimental results shown under chapter 5 a 7^{th} order inversion dependency to the PD rate was assumed, and a normalized PD rate (time constant) was calculated for varying degrees of inversion. Different applications, ranging from single-mode core pumped applications to cladding pumped high power (hundreds of Watts) were simulated, and the range of typical inversions obtained within the fiber are shown in Fig. 7.1. The figure illustrates the large dynamic range of the PD process; the lower inversion applications (cladding pumped cw lasers) typically operate at inversion levels <<10%, which implies that the fibers could operate without significant degradation for a long time period even with a core material that is susceptible to some degree of PD. Core pumped applications, however, exhibit typically a high inversion that is mainly defined by the pump wavelength, i.e. even cw laser cavities operate at relatively high inversion levels, and any susceptibility to PD should be evident as the device is taken to use. Measurement results made by different groups suggest that the rate is

dependent on glass composition and possibly manufacturing method [61,64]. This implies that the PD rate dependency should be experimentally verified for glasses of different composition or origin prior to estimating the lifetime based on inversion, application length, and other factors.

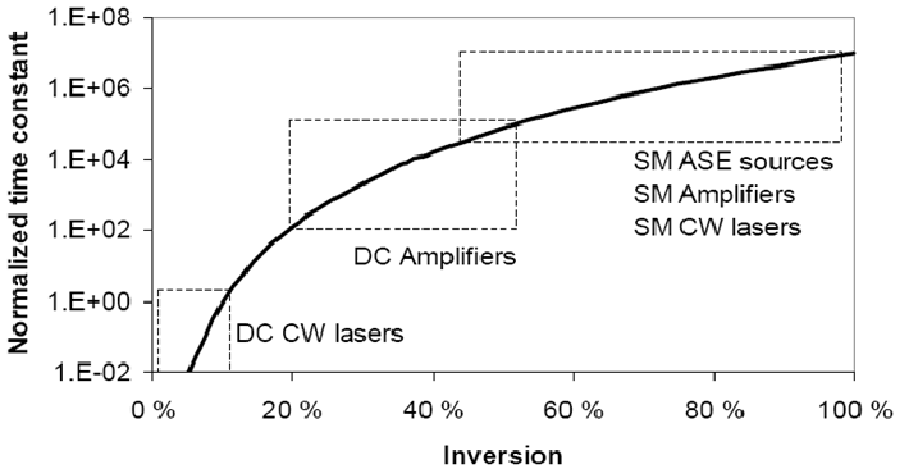

Figure 7.1. Normalized PD time constants for different applications operating at different inversion regimes, assuming the 7th order inversion dependency.

7.1 Radial distribution of photodarkening

In PD measurements that aim to benchmark or study the PD properties of fibers care was taken to induce as flat an inversion profile as possible

in order to obtain a transmission measurement that was representative throughout the sample length. In applications the inversion profile is rarely flat, and typically the inversion is time dependent as is the case for example in amplifiers operated on pulsed regime. For LMA fibers operated as spatially single-mode the mode-crunching phenomenon is of particular interest. As a fiber is bent, the effective refractive index profile of the fiber changes in a way that the outer edge of the fiber has a higher refractive index in comparison to the inner edge of the fiber, and subsequently the field distribution is shifted (or crunched) towards the outer edge of the bend [68]. This may have repercussions to fibers susceptibe to PD, as the spatial inversion profile of the fiber is inversely proportional to the signal power. The inversion behavior was demonstrated by Hotoleanu *et al.* [69] by simulations, and Söderlund *et al.* by experiments on visible wavelengths [70]. The demonstration of spatially distributed PD in an LMA fiber laser was the subject of publication V.

Simulation results for a specific fiber, namely with a 30 µm core and 0.07 NA, calculated with different coiling diameters are illustrated in Fig. 7.2. The fundamental mode of the fiber is seen to shift towards the outer edge of the coiling direction, and as coiling is increased the mode area is seen to decrease and with the smallest bending diameter a significant amount of light is seen to leak outside the core. Simulations were performed using a commercially available software Liekki Application Designer v3.3.

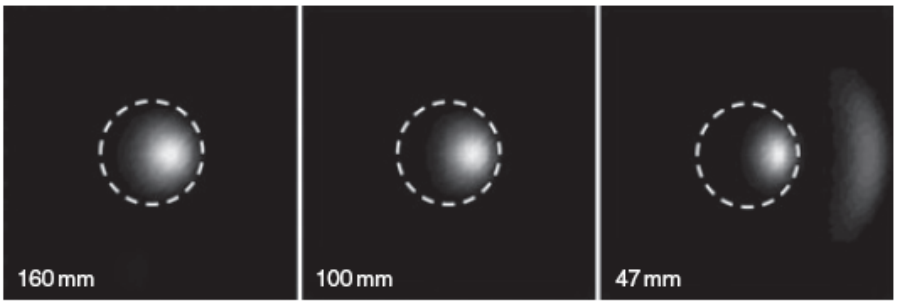

Figure 7.2. Simulated fundamental mode intensity profile for a 30 µm diameter core bent to varying coiling diameters. The dashed line is the edge of the 30 µm diameter core. Spatial inversion within the core is inversely proportional to the intensity.

Mode crunching induced PD was studied by measuring coiled fibers for their signal slope power conversion efficiency (PCE) from the absorbed pump power. The measurements were conducted by cleaving both ends of the fiber samples with flat cleaves, and using the Fresnel reflections as the mirrors for the fiber laser cavity. Output signal power from both ends was measured, and the non-absorbed pump power was also measured from the output end of the fiber, as shown in Fig. 7.3. The experiments were conducted on 30 µm core / 250 µm cladding diameter DC fibers, and the samples were coiled with diameters of 160 mm, 100 mm, and 47 mm to induce varying levels of mode crunching and higher order mode discrimination. The pump absorptions of the fiber samples were between 8-10 dB for the pump wavelengths of 920 nm and 980 nm, with 5 m and 3 m fiber lengths, respectively. The core and cladding NA's were 0.07 and 0.46,

respectively. The coupled pump power was up to 15 W, and the fiber laser cavities lased at wavelengths ranging from 1060 to 1080 nm with a wide emission spectrum. As the smallest coiling diameter induced significant losses also for the fundamental mode, the PCE values were normalized with the value of the pristine sample at each coiling diameter. The PCE values ranged from 35% (small coiling diameters) to 70% (larger diameters). Apertures were used to filter the signal light propagating in the cladding in order to measure only the losses to the signal propagating in the core.

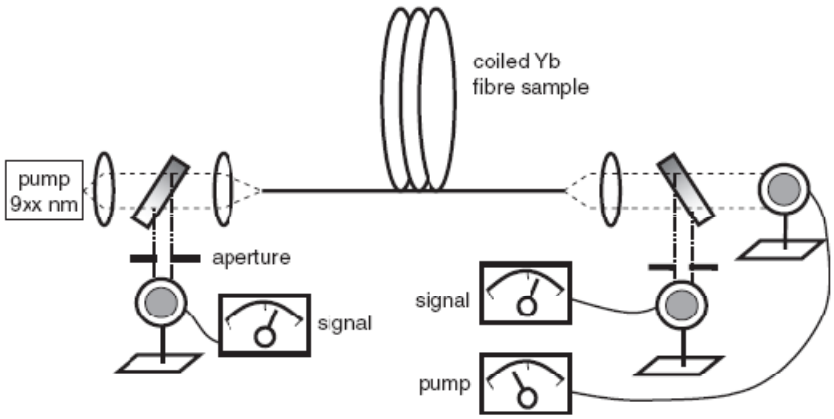

Figure 7.3. Measurement setup to study mode crunching induced PD. Signal was separated from pump using dichroic filters. Signal power from both ends of the fiber was measured, and the excess pump power out of the fiber was measured.

Each measurement consisted of the following steps:

1) Measuring the signal slope PCE from the absorbed pump of a pristine fiber sample.

2) Running the fiber laser in CW operation for 180 minutes to induce PD.

3) Measuring PCE for a 2nd time to verify that the CW lasing operation had not degraded the efficiency of the part of fiber in low inversion.

4) Recoiling the fiber to opposite direction to induce the mode crunching effect to a different part of the core. The fiber ends were fixed to reference planes during the recoiling, and the recoiling was done directly from one mandrel to another to minimize undesirable rotation of the fiber.

5) Measuring PCE for a 3rd time to observe the PD induced degradation of the region of the core that had high inversion during CW lasing.

Based on our results we assume that the PCE measurement was fast enough not to significantly affect the degree of PD in the fiber. We estimate the error of the resulting PCE values to be ± 3 normalised %-units.

The results from three different fiber samples measured with different coiling diameters are shown in Fig. 7.4. During the experiment no significant degradation was observed in the 2nd PCE measurement, as expected. In the smallest coiling diameter samples the mode crunching induced PD was observed after re-coiling, and resulted in a degradation of up to 20% from the original value. More measurements were conducted using the smallest coiling diameter, as shown in Fig. 7.5. Both pump wavelengths induced degradation in the part of fiber under high inversion. The smaller PCE degradation of the 980 nm pump wavelength case is attributed to a shorter sample length (yielding less total induced loss) and (based on simulations) approximately the same inversion profile. Sample 2 did not show significant degradation under the experimental conditions, we suspect this was due to lower inversion induced by spatially few-moded lasing.

The smallest coiling diameter shows significant mode crunching, leaving the dark part of the fiber in high inversion, as shown in Fig. 7.2. During the experiments the only method used to suppress higher-order modes was the one-directional coiling. Because of this the lasing in the cavity may have been spatially few-moded, which would partially suppress the inversion in the region which is shown as dark in Fig. 7.2. In a case of strictly singlemode operation (e.g in an amplifier with good launching conditions) we expect the effect to be more pronounced. To observe the effect one still has to re-coil the fiber in a way that the modal overlap changes within the core. Based on the

experimental results and simulations we estimate that the mode crunching induced PD effect will not be significant in cases where the core diameter is 30 µm (assuming 0.07 ± 0.01 NA) and the bending-induced spatial mode shift is smaller than half the modefield diameter of the fundamental mode. However, in larger diameter low NA fiber amplifiers that are coiled to near singlemode operation the effect may be of importance if the same fiber is coiled and re-coiled during experiments, and the core material of the fiber is susceptible to PD.

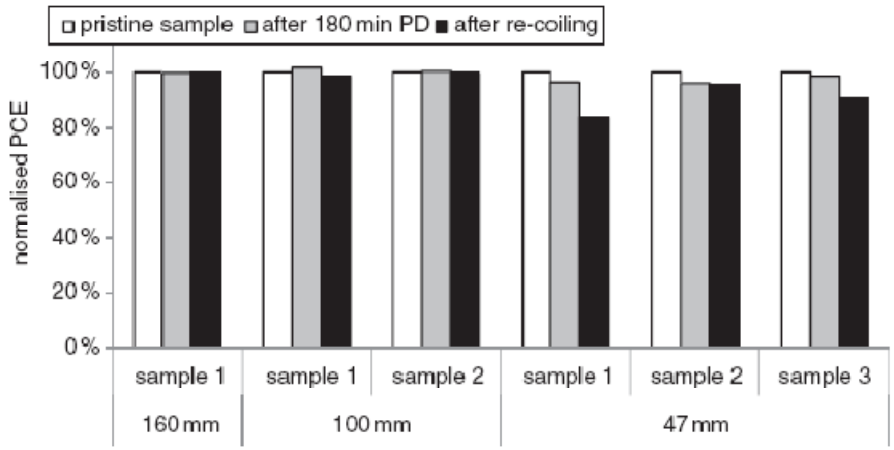

Figure 7.4. PCE results normalized to pristine fiber samples for different coiling diameters.

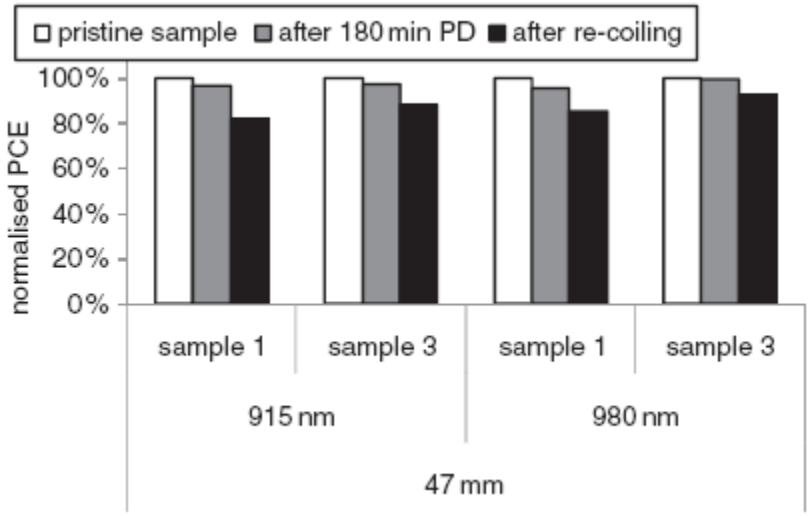

Figure 7.5. PCE results normalized to pristine fiber values for two different pump wavelengths at the smallest coiling diameter.

8 Summary

Prior to the early work described in this thesis no systematic study was performed and published on PD of Yb doped fibers. The interest in PD of Yb doped fibers was based on the need to increase the PD resistance of the doped fibers, and for this purpose a repeatable method to compare different fibers of varying compositions was required. The principal goal of this work was to develop a method for characterizing the PD propensity of fiber samples, and to obtain the results fast. The study of the driving mechanism behind PD became a subsequent goal of this work in order to further understand the implications of the PD in different applications.

A benchmarking measurement method was developed for single-mode fibers. The measurement method relied on inducing a flat and repeatable inversion level to the samples by saturating the inversion level. The loss measurements were conducted spectrally, and it was shown that the PD benchmarking, comparison, and study could be performed at shorter wavelengths (for example the HeNe wavelength of 633 nm) to improve the signal-to-noise ratio when compared to measurements conducted at the signal wavelengths (at 1030-1100 nm).

A method to induce a flat and variable inversion to Yb doped fibers was developed in order to study the temporal behavior of PD. The measurements conducted on DC Yb doped fiber samples revealed, that

the key driver behind PD rate is the inversion level induced in the doped glass. Two different methods to analyze the decay rate data were used: the stretched exponential method and the bi-exponential method. The stretched exponential method gave phenomenological means of quantifying the PD rate, and the bi-exponential method enabled describing the PD rate as the result of multiple exponential decay processes. The resultant PD rate constants can be parameterized in terms of single variable, the excited-state Yb concentration in the fiber. In addition to identifying the key controlling variable in PD, this result implies that a given glass composition can be characterized by a unique PD propensity. This propensity can be used to quantitatively compare different fibers, guide development of new fibers, and identify critical aspects of the fiber fabrication process control. Additionally, PD time constants were found to follow a simple power law and are proportional to $[Yb]^{*7\pm1}$, which suggests that ~7 Yb* ions in close proximity may be involved in the PD process. This very high-order dependence has significant implications for fiber devices, yielding orders of magnitude differences in the PD rate for dissimilar applications such as a cw cladding pumped lasers versus a high gain amplifier. The simple functional dependence for the PD rate on inversion may indicate a single, well-defined mechanism for color-center formation, although other physical processes cannot yet be ruled out.

Both the core pumping and the cladding pumping methods of inducing inversion were simulated to find the principal strengths and

weaknesses of both methods. The critical parameter defining the inversion in the core pumping method was found to be the pump wavelength, assuming pump irradiance above the saturation level of inversion are used. This property makes the induced inversion very repeatable, as methods to stabilize the wavelength are readily available with for example fiber Bragg gratings. To decrease the pump power required for inversion saturation, the pump wavelengths near 976 nm absorption peak are preferred. The cladding pumping method was found to have multiple critical parameters: pump power, pump wavelength, and sample length all have significant impact to the measured loss. Due to the above the core pumping method can be seen to be more suitable for benchmarking measurements, and the cladding pumping method more applicable for advanced studies of the PD phenomenon.

The radial distribution of PD was studied in an LMA fiber. The earlier simulation and measurement results were experimentally confirmed, and mode crunching induced PD in a cw fiber laser cavity was observed. The mode crunching induced PD effect may be of lesser importance in commercial applications where the fiber is not moved after packaging. The effect can, however, explain repeatability problems in experimental conditions where the same fiber may be coiled multiple times between experiments. The effect also needs to be taken into account when designing further methods of measuring PD from LMA fibers.

References

1. V. Gapontsev, D. Gapontsev, N. Platonov, O. Shkurikhin, V. Fomin, A. Mashkin, M. Abramov, and S. Ferin, "2 kW CW ytterbium fiber laser with record diffraction-limited brightness," in *Conference of Lasers and Electro-Optics / Europe*, CLEO/Europe Technical Digest (OSA, 2005), pp. 508.
2. Y. Jeong, J.K. Sahu, D.N. Payne, and J. Nilsson, "Ytterbium-doped large-core fiber laser with 1.36 kW continuous-wave output power," Opt. Express **12**, 6088-6092 (2004).
3. S. Norman, M. Zervas, A. Appleyard, P. Skull, D. Walker, Paul Turner, and Ian Crowe, "Power Scaling of High Power Fiber Lasers for Micromachining and Materials Processing Applications," Proc. SPIE **6102**, 61021P (2006).
4. M.N. Zervas, M. Durkin, F. Ghiringhelli, K. Vysniauskas, L. Hickey, A. Gillooly, P. Turner, B. Kao, "High peak power, high rep-rate pulsed fibre laser for marking applications," Proc. SPIE **6102**, 61020Q (2006).

5. S. Maryashin, A. Unt, and V. Gapontsev, “10 mJ pulse energy and 200 W average power Yb doped fiber laser,” Proc. SPIE **6102**, 61020O (2006).
6. J. Sillanpää, K. Ylä-Jarkko, and H. Asonen, ”Precise processing of Thin Films with picosecond Fiber Laser,” in Proceedings of Advanced Laser Applications Conference (2007).
7. www.fianium.com, FemtoPower1060-x-s, Product Datasheet (2008).
8. D.A.V. Kliner, F. Di Teodoro, J.P. Koplow, S.W. Moore, and A.V. Smith, “Efficient second, third, fourth, and fifth harmonic generation of a Yb-doped fiber amplifier,” Opt. Commun. **210**, 393-398 (2002).
9. N. Starodoumov; D. Dudley, S. McLean, A. Steinmetz, and N. Hodgson, “Hybrid fiber MOPA-bulk amplifier system for frequency conversion,” Proc. SPIE **6871**, 68710V (2008).
10. M. Kauf, R. Patel, J. Bovatsek, and W. Gries, “High power UV q-switched and mode-locked laser comparisons for industrial processing applications, “ Proc. SPIE **6871**, 687123 (2008).

11. A. Galvanauskas, M.-Y. Cheng, K.-C. Hou, and K.-H. Liao, “High Peak Power Pulse Amplification in Large-Core Yb-Doped Fiber Amplifiers”, IEEE J. Sel. Topics Quantum Electron. **13**, 559-566 (2007).
12. J. Limpert, O. Schmidt, J. Rothhardt, F. Röser, T. Schreiber, A. Tünnermann, S. Ermeneux, P. Yvernault, and F. Salin, “Extended single-mode photonic crystal fiber lasers,” Opt. Express **14**, 2715-2720 (2006).
13. R. Paschotta, J. Nilsson, P.R. Barber, J.E. Caplen, A.C. Tropper, and D.C. Hanna, “Lifetime quenching in Yb-doped fibres,” Opt. Comm. **136**, 375-378 (1997).
14. J. Koponen, M. Söderlund, S. Tammela, H. Po, ”Measuring photodarkening from Yb doped fibers,” in *Conference of Lasers and Electro-Optics / Europe*, CLEO/Europe Technical Digest (OSA, 2005), paper CP2-2-THU.
15. J. Hecht, “City of Light: The Story of Fiber Optics,” Oxford University Press (1999).
16. C.J. Koester, E. Snitzer, “Amplification in a Fiber Laser,” App. Opt. **3**, 1182-1186 (1964).

17. E. Snitzer, R. Woodcock, "Yb^{3+}-Er^{3+} Glass Laser," Appl. Phys. Lett. **6**, 45-46 (1965).

18. S.B. Poole, D.N. Payne, M.E. Fermann, "Fabrication of low-loss optical fibres containing rare-earth ions," El. Lett. **21**, 737-738 (1985).

19. J.E. Townsend, S.B. Poole, D.N. Payne, "Solution-doping technique for fabrication of rare-earth-doped optical fibers," El. Lett. **23**, 329-331 (1987).

20. E. Desurvire, J.R. Simpson, and P.C. Becker, "High-gain erbium-doped traveling-wave fiber amplifier," Opt. Lett. **12**, 888-890 (1987).

21. R.J. Mears, L. Reekie, I.M. Jauncey, and D.N. Payne, "Low-noise Erbium-doped fibre amplifier operating at 1.54μm," El. Lett. **23**, 1026-1028 (1987).

22. L. Philippe, V. Doya, R. Philippe, P. Dominique, M. Fabrice, and L. Olivier, "Experimental study of pump power absorption along rare-earth-doped double clad optical fibers," Opt. Comm. **218**, 249-254 (2003).

23. D. Kouznetsov, J.V. Moloney, and E.M. Wright, “Efficiency of pump absorption in double-clad fiber amplifiers. I. Fiber with circular symmetry,” J. Opt. Soc. Am. B **18**, 743-749 (2001).

24. D. Kouznetsov and J.V. Moloney, “Efficiency of pump absorption in double-clad fiber amplifiers. II. Broken circular symmetry,” J. Opt. Soc. Am. B **19**, 1259-1263 (2002).

25. E. Desurvire, J.L. Zyskind, and C.R. Giles, “Design Optimization for Efficient Erbium-Doped Fiber Amplifiers,” J. Lightwave Technol. **8**, 1730-1741 (1990).

26. J. Stone and C.A. Burrus, “Neodymium-doped silica lasers in end-pumped fiber geometry,” Appl. Phys. Lett. **23**, 388-389 (1973).

27. S. Jetschke, S. Unger, A. Schwuchow, M. Leich, and J. Kirchhof, “Efficient Yb laser fibers with low photodarkening by optimization of the core composition,” Opt. Exp. **16**, 15540-15545 (2008).

28. M. Engholm and L. Norin, “Preventing photodarkening in ytterbium-doped high power fiber lasers; correlation to the UV-transparency of the core glass,” Opt. Exp. **16**, 1260-1268 (2008).

29. A.H. Cherin, “An Introduction to Optical Fibers,” McGraw-Hill, Japan (1983).

30. D. Gloge, “Weakly guiding fibers,” Applied Optics **10**, 2252-2258 (1971).

31. M. Bass, J.M. Enoch, E.W.V. Stryland, W.L. Wolfe, “Handbook of Optics: Volume IV, Fiber Optics and Nonlinear Optics,” McGraw-Hill, New York, U.S. (2001).

32. W.J. Miniscalco, R.S. Quimby, “General procedure for the analysis of Er^{3+} cross sections,” Opt. Lett. **16**, 258-260 (1991).

33. D.E. McCumber, “Einstein Relations Connecting Broadband Emission and Absorption Spectra,” Phys. Rev. **136**, A954-A957 (1964).

34. P.C. Becker, N.A. Olsson, and J.R. Simpson, “Erbium-doped Fiber Amplifiers: Fundamentals and Technology,” Adademic Press (1999).

35. C.B. Layne, W.H. Lowdermilk, and M.J. Weber, “Multiphonon relaxation of rare-earth ions in oxide glasses,” Phys. Rev. B **16**, 10-20 (1976).

36. K. Arai, H. Namikawa, K. Kumata, and T. Honda, ”Aluminum or Phosphorus co-doping effects on the fluorescence and structural

properties of neodymium-doped silica glass," J. Appl. Phys. **59**, 3430-3436 (1986).

37. S.G. Kosinski, D.M. Krol, T.M. Duncan, D.C. Douglass J.B. MacChesney, and J.R. Simpson, "Raman and NMR Spectroscopy of SiO_2 glasses co-doped with Al_2O_3 and P_2O_5," J. Non-Cryst. Solids **105**, 45-52 (1988).
38. G.G. Vienne, W.S. Brocklesby, R.S. Brown, Z.J. Chen, J,D. Minelly, J.E. Roman, and D.N. Payne "Role of Aluminum in Ytterbium-Erbium Codoped Phosphoaluminosilicate Optical Fibers," Optical Fiber Technology **2**, 387-393 (1996).
39. B.J. Ainslie, "A Review of the Fabrication and Properties of Erbium-Doped Fibers for Optical Amplifiers," J. Lightwave Tech. **9**, 220-227 (1991).
40. R.P. Tumminnelli, B.C. McCollum, and E. Snitzer, "Fabrication of High-Concentration Rare-Earth Doped Optical Fibers Using Chelates," J. Lightwave Tech. **8**, 1680-1683 (1990).
41. P.C. Schultz, "Fabrication of Optical Waveguides by the Outside Vapor Deposition Process," Proc. of the IEEE **68**, 1187-1190 (1980).

42. L. Norin, E. Vanin, P. Soininen, and M. Putkonen, ”Atomic Layer Deposition as a New Method for Rare-Earth Doping of Optical Fibers,” Proc. of Conference on Lasers and Electro-Optics, CTuBB5 (2007).
43. S. Tammela, P. Kiiveri, S. Särkilahti, M. Hotoleanu, H. Valkonen, M. Rajala, J. Kurki, and K. Janka, ”Direct Nanoparticle Deposition process for manufacturing very short high gain Er-doped silica glass fibers,” Proc. European Conference on Optical Communications, Erbium Doped Fibers and Waveguides 9.4.2 (2002).
44. W.F. Smith, “Principles of Materials Science and Engineering,” McGraw-Hill, U.S. (1996).
45. A. Méndez and T.F. Morse, “Specialty Optical Fibers Handbook,” Academic Press, Elsevier, MA, USA (2007).
46. H. Po, E. Snitzer, R. Tumminnelli, L. Zenteno, F. Hakimi, N. Cho, and T. Haw, ”Double Clad High Brightness Nd Fiber Laser Pumped with GaAlAs Phased Array,” Proceedings of Optical Fiber Conference, PD7 (1989).

47. D.C.Hanna, H.M.Pask, J.E.Townsend, J.L.Archambault, L.Reekie, and A.C.Tropper, “An Yb-doped silica cladding-pumped fibre laser pumped at 974nm,” Proceedings 9th Topical Meeting on Advanced Solid-State Lasers, ATuB4 pp.143-145 (1994).

48. L. B. Glebov, “Linear and Nonlinear Photoionization of Silicate Glasses,” Glass Sci. Technol. **75,** C2 (2002).

49. D.C. Brown and H.J. Hoffman, “Thermal, stress, and thermo-optic effects in high average power double-clad silica fiber lasers,” IEEE J. Quantum Electron. **37**, 207-217 (2001).

50. P.E. Schrader, R.L. Farrow, D.A.V. Kliner, J.-P. Fève, and N. Landru, “Fiber-Based Laser with Tunable Repetition Rate, Fixed Pulse Duration, and Multiple Wavelength Output,” Proc. SPIE **6453** (2007).

51. M. Broer, D. M. Krol, and D. J. DiGiovanni, “Highly nonlinear near-resonant photodarkening in a thulium-doped aluminosilicate glass fiber,” Opt. Lett. **18,** 799-801 (1993).

52. I. J. Booth, J. L. Archambault, and B. F. Ventrudo, “Photodegradation of near-infrared-pumped Tm^{3+}-doped ZBLAN fiber upconversion laser,” Opt. Lett. **21**, 348-350 (1996).

53. G. R. Atkins and A. L. G. Carter, "Photodarkening in Tb^{3+}-doped phosphosilicate and germanosilicate optical fibers", Opt. Lett. **19**, 874-876 (1994).

54. M.M. Broer, R.L. Cone, and J.R. Sompson, "Ultraviolet-induced distributed-feedback gratings in Ce^{3+}-doped silica optical fibers," Opt. Lett. **16,** 1391-1393 (1991).

55. E.G. Behrens and R.C. Powell, "Characteristics of laser-induced gratings in Pr^{3+}- and Eu^{3+} -doped silicate glasses," J. Opt. Soc. Am. B **7,** 1437-1444 (1990).

56. S. Yoo, C. Basu, A. J. Boyland, C. Sones, J. Nilsson, J. K. Sahu, and D. Payne, "Photodarkening in Yb-doped aluminosilicate fibers induced by 488 nm irradiation," Opt. Lett. **32**, 1626-1628 (2007).

57. M. Engholm, L. Norin, and D. Åberg, "Strong UV absorption and visible luminescence in ytterbium-doped aluminosilicate glass under UV excitation," Opt. Lett. **32**, 3352-3354 (2007).

58. A.D. Guzman Chávez, A.V. Kir'yanov, Yu.O. Barmenkov, and N.N. Il'ichev, "Reversible photo-darkening and resonant photobleaching of Ytterbium-doped silica fiber at in-core 977-nm and 543-nm irradiation," Laser Phys. Lett. **4**, 10, 734–739 (2007).

59. T. Kitabayashi, M. Ikeda, M. Nakai, T. Sakai, K. Himeno, and K. Ohashi, "Population Inversion Factor Dependence of Photodarkening of Yb-doped Fibers and its Suppression by Highly Aluminum Doping," in *Conference of Lasers and Electro-Optics*, CLEO Technical Digest (OSA, 2006), paper OThC5.

60. B. Morasse, S. Chatigny, E. Gagnon, C. Hovington, J-P. Martin, and J-P. de Sandro, "Low photodarkening single cladding ytterbium fiber amplifier," Proc. SPIE **6453** (2007).

61. A.V. Shubin, M.V. Yashkov, M.A. Melkumov, S.A. Smirnov, I.A.Bufetov, and E.M.Dianov, "Photodarkening of alumosilicate and phosphosilicate Yb-doped fibers," in *Conference of Lasers and Electro-Optics / Europe*, CLEO/Europe Technical Digest (OSA, 2007), paper CJ3-1-THU.

62. J. Jasapara, M. Andrejco, D. DiGiovanni, and R. Windeler, "Effect of heat and H_2 gas on the photo-darkening of Yb^{+3} fibers," in *Conference of Lasers and Electro-Optics*, CLEO Technical Digest (OSA, 2006), paper CTuQ5.

63. I. Manek-Hönninger, J. Boullet, T. Cardinal, F. Guillen, S. Ermeneux, M. Podgorski, R. Bello Doua, and F. Salin,

"Photodarkening and photobleaching of an ytterbium-doped silica double-clad LMA fiber," Opt. Express **15,** 1606 (2007).

64. S. Jetschke, S. Unger, U. Röpke, and J. Kirchhof, "Photodarkening in Yb doped fibers: experimental evidence of equilibrium states depending on the pump power," Opt. Express **15**, 14838 (2007).
65. K.E. Mattson, S.N. Knudsen, B. Cadier, and T. Robin, "Photo darkening in ytterbium co-doped silica material", Proc. SPIE **6873**, 6873-48 (2008).
66. J.J. Koponen, M.J. Söderlund, S.K. Tammela, and H. Po, "Photodarkening in ytterbium-doped silica fibers," Proc. SPIE **5990**, 599008 (2005).
67. A. Chandonnet, P. Laperle, S. LaRochelle, and R. Vallée, "Photodegradation of fluoride glass blue fiber laser," in Photosensitive Optical Materials and Devices, Mark P. Andrews, Ed., Proc. SPIE **2998**, 70 (1997).
68. D. Marcuse, "Field deformation and loss caused by curvature of optical fibers," J. Opt. Soc. Am. **66**, 311-320 (1976).
69. M. Hotoleanu, J. Koponen, and T. Kokki, "Spatial distribution of photodarkening in large mode area Ytterbium doped fibers," in

Conference of Advanced Solid State Photonics, ASSP Technical Digest (OSA, 2008), paper WE23M.

70. M. Söderlund, J.J. Montiel i Ponsoda, S.K.T. Tammela, K. Ylä-Jarkko, A. Salokatve, S. Honkanen, ” Mode-induced transverse photodarkening loss variations in large-mode-area ytterbium doped silica fibers,” Opt. Express **16**, 10633-10640 (2008).

Attached publications

ISBN 978-951-22-9667-5
ISBN 978-951-22-9668-2 (PDF)
ISSN 1795-2239
ISSN 1795-4584 (PDF)